On Optimal Reconstruction of Constitutive Relations

Vladislav Bukshtynov [a], Oleg Volkov [b], and Bartosz Protas [b,*]

[a] *School of Computational Engineering and Science, McMaster University, Hamilton, Ontario, Canada*

[b] *Department of Mathematics & Statistics, McMaster University, Hamilton, Ontario, Canada*

Abstract

In this investigation we develop and validate a computational method for reconstructing constitutive relations based on measurement data and applicable to problems arising in nonequilibrium thermodynamics and continuum mechanics. This parameter estimation problem is solved as PDE–constrained optimization using a gradient–based technique in the optimize–then–discretize framework. The principal challenge is that the control variable (i.e., the relation characterizing the constitutive property) is not a function of the independent variables in the problem, but of the state (dependent) variable. The proposed method allows one to reconstruct a smooth constitutive relation defined over a broad range of the dependent variable. It relies on three main ingredients: a computationally friendly expression for the cost functional gradient, Sobolev gradients used in lieu of discontinuous L_2 gradients, and a systematic technique for shifting the identifiability region. Performance of this approach is illustrated by the reconstruction of the temperature dependence of the thermal conductivity in a one–dimensional model problem.

Key words: parameter estimation, constitutive relations, optimization, nonequilibrium thermodynamics, continuum mechanics, adjoint analysis
PACS: 47.10.ab, 05.70.Ln, 02.30.Zz

1 Introduction

Reliable mathematical and computational modelling of physical processes depends on our knowledge of the relevant properties of the materials involved. Obtaining such properties is particularly challenging when the materials are of a less common type. For example, when investigating

* Corresponding author. Email: bprotas@mcmaster.ca, Phone: +1 905 525 9140 ext. 24116, Fax: 905-522-0935

thermo–fluid phenomena occurring in liquid metals, one needs to know the coefficients of viscosity, thermal diffusivity, surface tension, etc., for the specific alloys. This task is often made more difficult by the fact that these coefficients tend to depend on the temperature in a complicated way. As a result, precise information about such material properties is rarely available, except for some common materials. The goal of this investigation is to propose and validate a computational method that will allow one to reconstruct such material properties based on some measurements available for a particular process (e.g., heat conduction) and a particular material. The specific motivation for this investigation comes from our research on optimization of multiphysics phenomena involved in advanced welding processes [1], where accurate data concerning material properties is quite important. While our intended applications concern more complicated systems, for the sake of clarity in this paper our approach is developed and validated based on a fairly simple model problem.

In principle, as regards the inverse problem of parameter estimation, one can consider two distinct formulations:

- material properties depending on the *space* variable $\mathbf{x}$ (i.e., the *independent* variable in the problem), and
- material properties depending on the *state* variable T (i.e., the *dependent* variable in the problem).

Problems of the first type have in fact received quite a lot of attention in the literature, and we refer the reader to the monographs [2] and [3,4] for surveys of the mathematical and more applied aspects of these problems, respectively. For example, as the reconstructed parameters are functions of the space variables, these problems represent the foundation of numerous imaging techniques in medical diagnostics, such as, e.g., X–ray tomography [4], as well as in geosciences [5]. Problems of this type are at least in principle relatively well understood, and there exist several established methods for their solution.

In this paper our focus will be exclusively on parameter estimation problems of the second type in which we want to determine the material properties as a function of the state (i.e., *dependent*) variable, e.g., the temperature T, rather than the position in space (the *independent* variable). In other words, we seek a relationship between the material property and the state variable that holds uniformly at *every* point $\mathbf{x}$ of the domain Ω in which the problem is formulated. This problem seems to have received less attention in the literature than the problem of estimating the space–dependent material properties. Foundations of an optimization–based approach to the solution of this problem were laid in the work of Chavent and Lemonnier [6] (which to the best of our knowledge never appeared in the English language), where the authors established the existence of solutions to the problem and derived expressions for the gradient of the least–squares error functional. They also showed the results of computations in which the cost functional gradients were obtained based on a suitably–defined adjoint system. Similar problems were also considered by Alifanov et al. [7,8], except that in their formulation the dependence of the material property on the state variable was assumed in the form of a spline interpolant, effectively resulting in a finite–dimensional optimization problem. A computational approach also based on a least–squares error functional and a linearization of the problem via a suitable change of variables was considered by Tai and Kärkkäinen [9]. An alternative technique utilizing the adjoint equations, but without making use of the error functional, was proposed by DuChateau

et al. [10], whereas Janicki and Kindermann studied a method combining Green's functions and Landweber's iteration applied to the parameter–to–measurements map [11]. A different approach, based on the "equation error method", was pursued by Hanke and Scherzer [12] who also considered a discrete formulation. Some mathematical aspects of the inverse problem of determining the state–dependent diffusion coefficients were addressed by Kügler [13,14] who investigated the Tikhonov regularization, by Neubauer [15] who studied regularization using adaptive grids and also by DuChateau et al. [16,17]. Some analytical results concerning this problem posed in an infinite domain were also reported in [18]. In the present investigation we consider an optimization–based approach to estimation of a state–dependent material property and the main contribution of our work are as follows

- we provide a novel expression for the gradient of the cost functional which is more computationally tractable than the formula originally derived in [6],
- recognizing that in the standard formulation (based on the L_2 inner products) the cost functional gradients may be discontinuous, we develop an approach ensuring a required degree of smoothness of the reconstructed material properties, and
- noting that in a given problem reconstruction is normally limited to the corresponding "identifiability region" (defined below), we propose a systematic experimental design procedure that allows one to tune inputs to the system, so that the constitutive relation can be reconstructed over a broader range of the state variable.

While adjoint analysis is now routinely used to solve partial differential equation (PDE)–constrained optimization problems [19], we emphasize that the structure of the gradients in the present problem is in fact quite different from what is encountered in typical problems [20]. The reason is that the optimization variable is a function of the dependent, rather than independent, variables in the problem. We also add that, in contrast to the results reported in some of the references quoted above, our approach is formulated in the "optimize–then–discretize" framework, i.e., while we ultimately discretize the problem for the purpose of a numerical solution, our optimality conditions and the cost functional gradients are derived in the continuous (PDE) setting. As a consequence, the main constituents of our approach are independent of the specific discretization used.

In order to ensure applicability of our proposed approach to a broad array of problems in continuum mechanics and nonequilibrium thermodynamics, we formulate it in terms of reconstruction of constitutive relations. Thus, we will consider optimal reconstruction of isotropic constitutive relationships between thermodynamic variables based on measurements obtained in a spatially–extended system. In other words, assuming the constitutive relation in the following general form

$$\begin{bmatrix}\text{thermodynamic}\\ \text{flux}\end{bmatrix} = k\,(\text{state variables}) \begin{bmatrix}\text{thermodynamic}\\ \text{“force”}\end{bmatrix}, \tag{1}$$

our approach allows us to reconstruct the dependence of the transport coefficient k on the state variables consistent with the assumed governing equations. Constitutive relations in form (1) arise in many areas of nonequilibrium thermodynamics and continuum mechanics. To fix attention, but without loss of generality, in the present investigation we focus on a heat conduction problem in which the heat flux $\mathbf{q}$ represents the thermodynamic flux, whereas the temperature

gradient $\boldsymbol{\nabla} T$ is the thermodynamic "force", so that relation (1) takes the specific form

$$\mathbf{q}(\mathbf{x}) = -k(T)\,\boldsymbol{\nabla} T(\mathbf{x}), \qquad \mathbf{x} \in \Omega, \tag{2}$$

where $\Omega \subset \mathbb{R}^n$, $n = 1, 2, 3$, is an open domain in which the problem is formulated. We note that by assuming the function $k : \mathbb{R} \to \mathbb{R}$ to be given by a constant, we recover the well–known linear Fourier law of heat conduction. While expressions for the transport coefficients such as $k(T)$ are typically obtained using methods of statistical thermodynamics, in the present investigation we will show how to reconstruct the function $k(T)$ based on some available measurements of the spatial distribution of the state variable T combined with the relevant conservation law. Such a technique could be useful, for example, to systematically adjust the form of a constitutive relationship derived theoretically to better match actual experimental data. Combining constitutive relation (2) with an expression for the conservation of energy, we obtain a partial differential equation describing the distribution of the temperature T in the domain Ω corresponding to the distribution of heat sources $g : \Omega \to \mathbb{R}$ and suitable boundary conditions (for example, of the Dirichlet type), i.e.,

$$-\boldsymbol{\nabla} \cdot [k(T)\,\boldsymbol{\nabla} T] = g \qquad \text{in } \Omega, \tag{3a}$$

$$T = T_0 \qquad \text{on } \partial\Omega, \tag{3b}$$

where T_0 denotes the boundary temperature. Instead of (3b), we could also consider Neumann boundary conditions involving $k(T)\frac{\partial T}{\partial n}$, where $\mathbf{n}$ is the unit vector normal to the boundary $\partial\Omega$ and pointing out of the domain, and our subsequent analysis would essentially be unchanged. In regard to reconstruction of constitutive relations, it is important that such relations be consistent with the second principle of thermodynamics [21]. There exist two mathematical formalisms, one due to Coleman and Noll [22] and another one due to Liu [23], developed to ensure in a very general setting that a given form of the constitutive relation does not violate the second principle of thermodynamics. In continuous thermodynamical and mechanical systems this principle is expressed in terms of the Clausius–Duhem inequality [24] which in the case of the present simple model problem (2)–(3) reduces to the statement that $k(T) > 0$ for all values of T. At the same time, the condition $k(T) > 0$ is also required for the mathematical well–posedness of elliptic boundary value problem (3). In addition, to ensure the existence of classical (strong) solutions of (3), we will assume that the heat source $g(\mathbf{x}) > 0$ is at least a continuous function of $\mathbf{x}$. This appears reasonable taking into account possible physical phenomena represented by this term. The positivity of g allows us to establish a lower bound on classical solutions of problem (3), cf. Appendix A.

We now define two intervals:

- $[T_\alpha, T_\beta] \triangleq [\min_{\mathbf{x}\in\overline{\Omega}} T(\mathbf{x}), \max_{\mathbf{x}\in\overline{\Omega}} T(\mathbf{x})]$ which represents the range spanned by the solution of problem (3); we note that, as demonstrated in Appendix A, the minimum T_α is attained at the boundary $\partial\Omega$; following [14], we will refer to the interval $\mathcal{I} \triangleq [T_\alpha, T_\beta]$ as the *identifiability interval*,
- $\mathcal{L} \triangleq [T_a, T_b]$, where $T_a \leq T_\alpha$ and $T_b \geq T_\beta$; this will be the interval on which we will seek to obtain a reconstruction of the constitutive relation; we note that in general the interval $\mathcal{L}$ will be larger than the identifiability interval, i.e., $\mathcal{I} \subseteq \mathcal{L}$.

It is assumed that the constitutive relations $k(T)$ are differentiable functions of the state variable

(temperature) and belong to the following set

$$\mathcal{K} = \{k(T) \text{ piecewise } C^1 \text{ on } \mathcal{L};\ 0 < m_k < k(T) < M_k,\ \forall\, T \in \mathcal{L}\}, \tag{4}$$

where $m_k, M_k \in \mathbb{R}^+$, whereas solutions of problem (3) belong to $H^1(\Omega)$, i.e., the Sobolev space of functions defined on Ω with square–integrable derivatives.

The specific parameter estimation problem that we address in this investigation is formulated as follows. Given a set of continuous "measurements" $\tilde{T}(\mathbf{x})$, $\mathbf{x} \in \Sigma$, of the state variable (temperature) T acquired on the sensing domain $\Sigma \subseteq \Omega$, we seek to reconstruct the constitutive relation $k(T)$ for $T \in \mathcal{L}$ such that the solutions of problem (3) obtained with this reconstructed function $k(T)$ will best match the available measurements in the least–squares sense. Therefore, the constitutive relation $k(T)$ can be regarded as the "cause", whereas the measurements of the temperature field as the "effect". The general reconstruction problem is set up here based on continuous measurements, as required for consistency with the PDE–based formulation of the optimization problem. However, when we perform actual computations based on discretized PDEs, continuous measurements will be expressed in terms of suitable pointwise measurements which are more relevant from the application point of view. While our main goal in this investigation is to develop an efficient computational algorithm for this problem, some basic mathematical results concerning differentiability of the system outputs (measurements) with respect to the constitutive relation are recalled in an Appendix. Parameter estimation problems in general tend to be ill–posed [3], in the sense that measurement noise usually results in instabilities of the computed solutions. Therefore, we will analyze the performance of our method in the presence of noise, and will also assess the efficiency of Tikhonov regularization.

The plan of the paper is as follows: in the next Section we cast this parameter estimation problem as PDE–constrained optimization, in the following Section we show how the gradients of the cost functional can be conveniently computed using adjoint variables, whereas in Section 4 we outline some regularization strategies needed in the presence of measurement noise; in Section 5 we describe an experimental design procedure allowing one to adjust the system inputs in order to move the identifiability interval $\mathcal{I}$; in Section 6 we present a range of computational results, whereas summary and conclusions are deferred to Section 7. A number of theoretical results is collected in two Appendices.

2 Parameter Estimation as an Optimization Problem

We will assume that the set $\mathcal{K}$ consisting of constitutive relations $k(T)$ defined on $\mathcal{L}$ is embedded in a Hilbert (function) space $\mathcal{X}$ to be specified below. Solving our parameter estimation problem is therefore equivalent to finding a solution to the operator equation

$$\mathcal{F}(k) = T, \tag{5}$$

where $\mathcal{F} : \mathcal{K} \to L_2(\Sigma)$ is the map from the constitutive relations to the measurements. An approach commonly used to solve such problems consists in reformulating them as least–squares minimization problems which in the present case can be done by defining the cost functional

$\mathcal{J} : \mathcal{X} \to \mathbb{R}$ as

$$\mathcal{J}(k) \triangleq \frac{1}{2} \int_{\Sigma} \left[\tilde{T}(\mathbf{x}) - T(\mathbf{x}; k) \right]^2 \, d\mathbf{x}, \tag{6}$$

where the dependence of the temperature field $T(\cdot; k)$ on the form of the constitutive relation $k = k(T)$ is given by governing equation (3), and "$\triangleq$" means "equal to by definition". We will find minimizers of (6) using methods of gradient–based optimization and the required differentiability of map (5) with respect to k when $\mathcal{X} = H^1(\mathcal{I})$ is established in Appendix B. The optimal reconstruction $\hat{k}$ is therefore obtained as an unconstrained minimizer of cost functional (6), i.e.,

$$\hat{k} = \operatorname*{argmin}_{k \in \mathcal{X}} \mathcal{J}(k). \tag{7}$$

It is characterized by the first–order optimality condition which requires the directional differential of cost functional $\mathcal{J}$, defined as $\mathcal{J}'(k; k') = \lim_{\epsilon \to 0} \epsilon^{-1} [\mathcal{J}(k + \epsilon k') - \mathcal{J}(k)]$, to vanish for all perturbations $k' \in \mathcal{X}$ [25], i.e.,

$$\forall_{k' \in \mathcal{X}} \qquad \mathcal{J}'(\hat{k}; k') = 0. \tag{8}$$

The (local) optimizer $\hat{k}$ can be computed with the following gradient descent algorithm as $\hat{k} = \lim_{n \to \infty} k^{(n)}$, where

$$\begin{cases} k^{(n+1)} = k^{(n)} - \tau^{(n)} \boldsymbol{\nabla}_k \mathcal{J}(k^{(n)}), & n = 1, \ldots, \\ k^{(1)} \quad = k_0, \end{cases} \tag{9}$$

in which $\boldsymbol{\nabla}_k \mathcal{J}(k)$ represents the *gradient* of cost functional $\mathcal{J}(k)$ with respect to the control variable k (we will adopt the convention that a subscript on the operator $\boldsymbol{\nabla}$ will be used when differentiation is performed with respect to variables other than $\mathbf{x}$), $\tau^{(n)}$ is the length of the step along the descent direction at the n–th iteration, whereas k_0 is the initial guess taken, for instance, as a constant corresponding to a linear version of constitutive relation (2), or some other approximate theoretical prediction. For the sake of clarity, formulation (9) represents the steepest–descent algorithm, however, in practice one typically uses more advanced minimization techniques, such as the conjugate gradient method, or one of the quasi–Newton techniques [26]. We note that, since minimization problem (6)–(7) is in general nonconvex, condition (8) characterizes only a *local*, rather than *global*, minimizer. We reiterate that the constitutive property is required to satisfy the additional positivity condition $k(T) > 0$ for all $T \in \mathcal{L}$. Therefore, to be more precise, the optimal reconstruction $\hat{k}$ should be obtained as an *inequality*–constrained minimizer of cost functional (6), i.e.,

$$\hat{k} = \operatorname*{argmin}_{\substack{k \in \mathcal{X}, \\ k(T) > 0, \ T \in \mathcal{L}}} \mathcal{J}(k). \tag{10}$$

We add that in problems involving constitutive relations depending on several state variables the inequality constraint $k(T) > 0$ will be replaced with a more general form of the Clausius–Duhem inequality [24]. Inequality–constrained problem (10) can be transformed to an unconstrained formulation analogous to (7) using for example the barrier function approach [27]. Other computational techniques for solution of inequality–constrained parameter estimation problems are discussed in [28]. However, in the computational studies performed for our model problem and reported in Section 6 all solutions we found satisfied the condition $k(T) > 0$, $\forall T \in \mathcal{L}$, without having to enforce this condition explicitly. Hence, this issue will not be considered in the

present work, although we do intend to revisit it in the future in the context of more complicated problems.

3 Cost Functional Gradients via Adjoint–based Analysis

The key ingredient of minimization algorithm (9) is computation of the cost functional gradient $\boldsymbol{\nabla}_k \mathcal{J}(k)$. We emphasize that, since $k = k(T)$ is a continuous variable, the gradient $\boldsymbol{\nabla}_k \mathcal{J}(k)$ represents in fact an infinite–dimensional sensitivity of $\mathcal{J}(k)$ to perturbations of $k(T)$. Since our constitutive relations belong to set $\mathcal{K}$, cf. (4), we will seek to reconstruct $k(T)$ as elements of the Sobolev space $H^1(\mathcal{L})$, so that the gradient $\boldsymbol{\nabla}_k \mathcal{J}$ will need to be obtained with respect to the corresponding inner product. However, in order to make the derivation procedure easier to follow, we will first obtain an expression for the gradient in the space $L_2(\mathcal{L})$, and only then will obtain the Sobolev gradients which will be eventually used in the solution of optimization problem (7). In both steps our transformations will be formal. We begin by computing the directional differential of cost functional (6) which yields

$$\mathcal{J}'(k;k') = \int_\Sigma [T(\mathbf{x};k) - \tilde{T}(\mathbf{x})]\, T'(\mathbf{x};k,k')\, d\mathbf{x}, \tag{11}$$

where the perturbation variable $T'(\mathbf{x}_i;k,k')$ satisfies the perturbation system obtained from (3). Next, we invoke the Riesz representation theorem [30] for the directional differential $\mathcal{J}'(k;\cdot)$, which yields

$$\mathcal{J}'(k;k') = \langle \boldsymbol{\nabla}_k \mathcal{J}, k' \rangle_{\mathcal{X}}, \tag{12}$$

where $\langle \cdot,\cdot \rangle$ represents an inner product in the Hilbert space $\mathcal{X}$ (we will first set $\mathcal{X} = L_2(\mathcal{L})$ and afterwards change that to $\mathcal{X} = H^1(\mathcal{L})$). We note that the expression on the right–hand side (RHS) in (11) is not consistent with Riesz representation (12), since the perturbation variable k' is hidden in the system defining $T'(k,k')$. However, this expression can be transformed to Riesz form (12) with the help of a suitably–defined adjoint variable. Since our derivation of this result for the present problem is in fact quite different from the approach followed in [6], we state it in the form of the following theorem.

Theorem 3.1 *Let Ω be a smooth bounded open set and $k' \in \mathcal{X} = L_2(\mathcal{L})$. We assume that the function g and the solution T of* (3) *are sufficiently smooth. Then, the Riesz representation of directional differential* (11) *has the form*

$$\mathcal{J}'(k;k') = \int_{T_a}^{T_b} \left[\int_\Omega \chi_{[T_\alpha, T(\mathbf{x})]}(s) \Delta T^*\, d\mathbf{x} - \int_{\partial\Omega} \chi_{[T_\alpha, T(\mathbf{x})]}(s) \frac{\partial T^*}{\partial n}\, d\sigma \right] k'(s)\, ds, \tag{13}$$

where $\chi_{[a,b]}(s)$ is the characteristic function for an interval $[a,b]$ defined as follows

$$\chi_{[a,b]}(s) = \begin{cases} 1, & s \in [a,b], \\ 0, & s \notin [a,b], \end{cases}$$

whereas the adjoint state T^* is defined as the solution of the system

$$k(T)\boldsymbol{\Delta}T^* = [\tilde{T}(\mathbf{x}) - T(\mathbf{x})]\chi_\Sigma(\mathbf{x}), \qquad \textit{in } \Omega, \tag{14a}$$

$$T^* = 0, \qquad \textit{on } \partial\Omega, \tag{14b}$$

where

$$\chi_\Sigma(\mathbf{x}) = \begin{cases} 1, & \mathbf{x} \in \Sigma, \\ 0, & \mathbf{x} \notin \Sigma, \end{cases}$$

denotes the characteristic function of the sensing domain Σ.

PROOF. While in principle the proof could be formulated based on the original form of governing system (3), the derivation and structure of the resulting expressions for the gradient $\boldsymbol{\nabla}_k \mathcal{J}$ are simplified by a change of variables known as the "Kirchhoff transformation" [29]. We thus introduce an auxiliary function $V : \mathcal{I} \to \mathbb{R}$ defined as follows

$$V(T) \triangleq \int_{T_\alpha}^{T} k(s)\, ds. \tag{15}$$

Noting that in fact $T = T(\mathbf{x})$, we have $\boldsymbol{\nabla}V(\mathbf{x}) = k(T(\mathbf{x}))\, \boldsymbol{\nabla}T(\mathbf{x})$, and governing system (3) can be expressed as

$$-\boldsymbol{\Delta}V = g \qquad \text{in } \Omega, \tag{16a}$$

$$V(\mathbf{x}) = \int_{T_\alpha}^{T_0(\mathbf{x})} k(s)ds \qquad \text{on } \partial\Omega. \tag{16b}$$

(Using one symbol V to denote functions depending on T and $\mathbf{x}$ admittedly represents an abuse of notation, yet is justified here by simplicity.) Let $T^* : \Omega \to \mathbb{R}$ be an adjoint variable. We integrate (16a) against T^* to obtain

$$-\int_\Omega (\boldsymbol{\Delta}V)\, T^* d\mathbf{x} = \int_\Omega g\, T^* d\mathbf{x},$$

and then integrating by parts we get

$$\int_\Omega \boldsymbol{\nabla}V \cdot \boldsymbol{\nabla}T^*\, d\mathbf{x} - \int_{\partial\Omega} \frac{\partial V}{\partial n}\, T^*\, d\sigma = \int_\Omega g\, T^* d\mathbf{x}. \tag{17}$$

Next we differentiate (17) with respect to k

$$\int_\Omega \boldsymbol{\nabla}V' \cdot \boldsymbol{\nabla}T^* d\mathbf{x} - \int_{\partial\Omega} \frac{\partial V'}{\partial n} T^* d\sigma = 0,$$

where the perturbation variable V' can be expressed as [cf. (15)]

$$V'(T) = \int_{T_\alpha}^{T} k'(s)\, ds + k(T)T'(k, k'), \tag{18}$$

so that after integrating by parts one more time we obtain

$$\begin{aligned} &- \int_\Omega \left[\int_{T_\alpha}^{T(\mathbf{x})} k'(s) ds \right] \Delta T^* d\mathbf{x} - \int_\Omega k(T) T' \Delta T^* d\mathbf{x} \\ &+ \int_{\partial\Omega} \left[\int_{T_\alpha}^{T(\mathbf{x})} k'(s) ds + k(T) T' \right] \frac{\partial T^*}{\partial n} d\sigma - \int_{\partial\Omega} \frac{\partial V'}{\partial n} T^* d\sigma = 0. \end{aligned} \tag{19}$$

We now require that the adjoint variable T^* satisfy system (14). We note that owing to the judicious choice of the RHS term in (14a), the second term in relation (19) is in fact equal to the directional differential $\mathcal{J}'(k;k')$, so that we have

$$\mathcal{J}'(k;k') = \int_\Omega \left[\int_{T_\alpha}^{T(\mathbf{x})} k'(s)\, ds \right] \Delta T^*\, d\mathbf{x} - \int_{\partial\Omega} \left[\int_{T_\alpha}^{T(\mathbf{x})} k'(s)\, ds \right] \frac{\partial T^*}{\partial n} d\sigma. \tag{20}$$

We also notice that the boundary terms in (19) having T' and T^* as factors vanish due to the boundary conditions on the state and adjoint variables, respectively, (3b) and (14b). Finally, expression (13) for the Riesz representation of directional differential (11) can be obtained from (20) using the characteristic function $\chi_{[T_\alpha, T(\mathbf{x})]}(s)$ and reversing the order of integration with respect to $\mathbf{x}$ and s, where this last step is justified by Fubini's theorem. □

With the Riesz representation established in (13), we now proceed to identify expressions for the cost functional gradient $\boldsymbol{\nabla}_k \mathcal{J}$ according to (12). While this is not the gradient that we will use in actual computations, we analyze first the "simplest" case when $\mathcal{X} = L_2(\mathcal{L})$, i.e., the space of functions square integrable on $[T_a, T_b]$, as it already offers some interesting insights into the structure of the problem. The L_2 gradient of the cost functional hence takes the form

$$\boldsymbol{\nabla}_k^{L_2} \mathcal{J}(s) = \int_\Omega \chi_{[T_\alpha,\, T(\mathbf{x})]}(s) \Delta T^*\, d\mathbf{x} - \int_{\partial\Omega} \chi_{[T_\alpha,\, T(\mathbf{x})]}(s) \frac{\partial T^*}{\partial n}\, d\sigma. \tag{21}$$

We will now show that (21) is in fact equivalent to the cost functional gradient derived by Chavent and Lemonnier in [6] and adapted to the present time–independent problem. Let us consider the differentiation in (21) in the sense of distributions. Integration by parts of the first term on the RHS in (21) and the resulting cancellation of the second term yield

$$\boldsymbol{\nabla}_k^{L_2} \mathcal{J}(s) = - \int_\Omega \nabla \chi_{[T_\alpha,\, T(\mathbf{x})]}(s) \cdot \nabla T^*\, d\mathbf{x}. \tag{22}$$

The characteristic function $\chi_{[T_\alpha, T(\mathbf{x})]}(s)$ is a combination of Heaviside functions with respect to T. Therefore, its distributional derivative with respect to $\mathbf{x}$ can be expressed using the chain rule and a Dirac delta function as follows

$$\boldsymbol{\nabla}_k^{L_2} \mathcal{J}(s) = - \int_\Omega \delta(T(\mathbf{x}) - s)\, \nabla T \cdot \nabla T^*\, d\mathbf{x} = \frac{d}{ds} \int_\Omega \chi_{[T_\alpha, T(\mathbf{x}) - s]}(s)\, \nabla T \cdot \nabla T^*\, d\mathbf{x} \tag{23}$$

which is essentially the form of the cost functional gradient obtained in [6]. We note that the expression on the RHS in (23) involves differentiation of an integral with respect to the level set defining the integration region, an operation that is rather difficult to perform accurately in

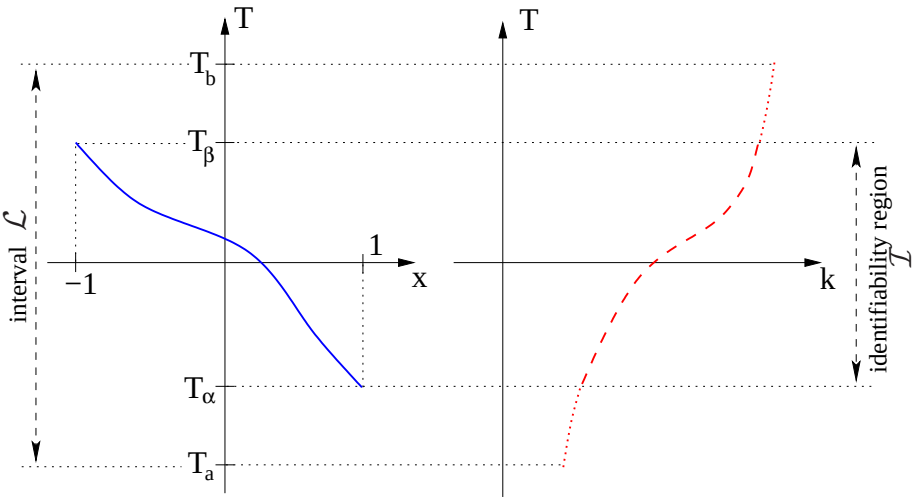

Fig. 1. Schematic showing (left) the solution $T(x)$ of governing system (3) and (right) the corresponding constitutive relation $k(T)$ defined over their respective domains, i.e., $\Omega = (-1, 1)$ and the identifiability region $\mathcal{I}$. The thick dotted line represents the extension of the the constitutive relation $k(T)$ from $\mathcal{I}$ to the interval $\mathcal{L}$. In the figure on the right the horizontal axis is to be interpreted as the ordinate.

numerical computations. Using (14a) we can transform expression for cost functional gradient (21) to a form more convenient from the point of view of numerical computations, namely

$$\boldsymbol{\nabla}_k^{L_2}\mathcal{J}(s) = \int_\Sigma \chi_{[T_\alpha,\, T(\mathbf{x})]}(s)\frac{\tilde{T}(\mathbf{x}) - T(\mathbf{x})}{k(T(\mathbf{x}))}\, d\mathbf{x} - \int_{\partial\Omega} \chi_{[T_\alpha,\, T(\mathbf{x})]}(s)\frac{\partial T^*}{\partial n}\, d\sigma, \tag{24}$$

where the numerical differentiation (with respect to $\mathbf{x}$) is only required in the second integral term.

The L_2 gradients have been used in numerous computational studies involving PDE–constrained optimization problem. In regard to the possibility of using the gradient $\boldsymbol{\nabla}_k^{L_2}\mathcal{J}$ in the computations for the present problem, the following comments are in place:

(1) gradient (21), or (24), is nonvanishing for $s \in \mathcal{I}$, and therefore the sensitivity of the functional $\mathcal{J}(k)$ to perturbations of k can only be determined on the identifiability region $\mathcal{I}$ which is typically smaller than the region $\mathcal{L}$ over which one would wish to reconstruct the constitutive relation; the relationships between the interval $\mathcal{L}$ and the identifiability region $\mathcal{I}$, the physical and the state spaces are illustrated in Figure 1 where we assumed $\Omega = (-1, 1)$,
(2) in view of the structure of expression (24), the L_2 gradient $\boldsymbol{\nabla}_k^{L_2}\mathcal{J}$ is in general a discontinuous function.

Evidently, in view of the issues mentioned above, the L_2 gradients are unsuitable for the reconstruction of the constitutive relations with the required properties, cf. (4). We will show that these difficulties can be overcome using cost functional gradients defined in the Sobolev space consistent with the functional setting of the problem, here $H^1(\mathcal{L})$ [31,32]. Such gradients are guaranteed to be sufficiently smooth and are obtained in a straightforward way from the L_2 gradients. Furthermore, these gradients can be defined on the entire interval $[T_a, T_b]$ without an artificial extension by zero and can be naturally combined with a technique to shift the identi-

fiability region. The Sobolev gradients are discussed below, whereas shifting the identifiability region is introduced in Section 5.

When defining Sobolev gradients in a PDE–constrained optimization problem one needs to specify suitable boundary conditions characterizing the behavior of the gradient on the boundary of its domain of definition. In "classical" problems in which the control parameter is a function of the independent variables in the problem, the choice of these boundary conditions usually follows quite naturally from the structure of the governing PDE. This is, however, not the case in the present problem where it is not obvious what behavior should be imposed on the gradient at the limits of the interval $\mathcal{L}$. Out of several different possibilities, we choose to examine the following two approaches.

In the first approach we construct the Sobolev gradients $\boldsymbol{\nabla}_k^{H^1}\mathcal{J}$ by assuming that $\mathcal{X} = H^1(\mathcal{L})$, where the Sobolev space $H^1(\mathcal{L})$ is endowed with the following inner product

$$\langle z_1, z_2\rangle_{H^1(\mathcal{L})} = \int_{T_a}^{T_b}\left[z_1 z_2 + l^2\frac{dz_1}{ds}\frac{dz_2}{ds}\right]ds, \qquad z_1, z_2 \in H^1(\mathcal{L}) \tag{25}$$

in which $l \in \mathbb{R}$ is a parameter with the meaning of a length–scale [we note that the L_2 inner product is obtained by setting $l = 0$ in (25)]. Next, we again invoke the Riesz representation theorem, however, now we assume that $k' \in H^1(\mathcal{L})$, so that we obtain

$$\mathcal{J}'(k;k') = \langle\boldsymbol{\nabla}_k^{L_2}\mathcal{J}, k'\rangle_{L_2(\mathcal{L})} = \langle\boldsymbol{\nabla}_k^{H^1}\mathcal{J}, k'\rangle_{H^1(\mathcal{L})} = \int_{T_a}^{T_b}\left[\boldsymbol{\nabla}_k^{H^1}\mathcal{J}\,k'(s) + l^2\frac{d(\boldsymbol{\nabla}_k^{H^1}\mathcal{J})}{ds}\frac{dk'}{ds}\right]ds. \tag{26}$$

Performing integration by parts and imposing the homogeneous Neumann boundary conditions on the Sobolev gradient, i.e., $\frac{d}{ds}\boldsymbol{\nabla}_k^{H^1}\mathcal{J}\big|_{T_a,T_b} = 0$, we obtain

$$\mathcal{J}'(k;k') = \int_{T_a}^{T_b}\boldsymbol{\nabla}_k^{L_2}\mathcal{J}\,k'(s)\,ds = \int_{T_a}^{T_b}\left[\boldsymbol{\nabla}_k^{H^1}\mathcal{J} - l^2\frac{d^2}{ds^2}\boldsymbol{\nabla}_k^{H^1}\mathcal{J}\right]k'(s)\,ds. \tag{27}$$

Noting that relation (27) must be satisfied for any arbitrary k', we conclude that the Sobolev gradient $\boldsymbol{\nabla}_k^{H^1}\mathcal{J}$ can be determined as a solution of the following inhomogeneous elliptic boundary–value problem

$$\boldsymbol{\nabla}_k^{H^1}\mathcal{J} - l^2\frac{d^2}{ds^2}\boldsymbol{\nabla}_k^{H^1}\mathcal{J} = \boldsymbol{\nabla}_k^{L_2}\mathcal{J} \qquad \text{on } (T_a, T_b), \tag{28a}$$

$$\frac{d}{ds}\boldsymbol{\nabla}_k^{H^1}\mathcal{J} = 0 \qquad \text{for } s = T_a, T_b. \tag{28b}$$

On the other hand, in the second approach we construct the Sobolev gradients $\boldsymbol{\nabla}_k^{H^1}\mathcal{J}$ by first assuming that $\mathcal{X} = H^1(\mathcal{I})$, where the Sobolev space $H^1(\mathcal{I})$ is endowed with an inner product analogous to (25), except that integration is now from T_α to T_β. Proceeding as above and imposing the homogeneous Neumann boundary conditions at the end points of the identifiability interval $\mathcal{I}$ we obtain the gradient $\boldsymbol{\nabla}_k^{H^1}\mathcal{J}$ as a solution of the following inhomogeneous elliptic

boundary–value problem

$$\boldsymbol{\nabla}_k^{H^1}\mathcal{J} - l^2\frac{d^2}{ds^2}\boldsymbol{\nabla}_k^{H^1}\mathcal{J} = \boldsymbol{\nabla}_k^{L_2}\mathcal{J} \qquad \text{on } (T_\alpha, T_\beta), \tag{29a}$$

$$\frac{d}{ds}\boldsymbol{\nabla}_k^{H^1}\mathcal{J} = 0 \qquad \text{for } s = T_\alpha, T_\beta. \tag{29b}$$

In order to be able to reconstruct the relation $k(T)$ over the entire interval $\mathcal{L}$ we need to extend the Sobolev gradient defined in (29) onto $\mathcal{L}$. We do this by prescribing

$$\boldsymbol{\nabla}_k^{H^1}\mathcal{J}(s) = \boldsymbol{\nabla}_k^{H^1}\mathcal{J}(T_\alpha) \qquad \text{for } s \in [T_a, T_\alpha], \tag{30a}$$

$$\boldsymbol{\nabla}_k^{H^1}\mathcal{J}(s) = \boldsymbol{\nabla}_k^{H^1}\mathcal{J}(T_\beta) \qquad \text{for } s \in [T_\beta, T_b] \tag{30b}$$

which preserves the continuity of the Sobolev gradient. Extraction of gradients in spaces of smoother functions, such as the Sobolev spaces considered here, is a well–known device in adjoint–based optimization of PDEs [32,33] where it is often regarded as a form of preconditioning. We also emphasize that by changing the value of the length–scale parameter l we can control the smoothness of the gradient $\boldsymbol{\nabla}_k^{H^1}\mathcal{J}(k)$, and therefore also the relative smoothness of the resulting reconstruction of $k(T)$. More specifically, it was shown in [32] that extracting cost functional gradients in the Sobolev spaces such as introduced above is equivalent to applying a low–pass filter to the L_2 gradient with the quantity l^{-2} representing the "cut-off" scale. In Section 6 we will compare the computational performance of the two approaches proposed and will discuss certain additional reasons why Sobolev gradients are a useful device for the present problem.

4 Reconstruction in the Presence of Measurement Noise

In this Section we discuss the important issue of reconstruction in the presence of noise in the measurements. As can be expected based on the general properties of parameter estimation problems [3], and as will be confirmed in Section 6.3, incorporation of random noise in the measurements leads to an instability in the form of small–scale oscillations appearing in the reconstructed constitutive relations. In the optimization framework a standard approach to mitigate this problem is Tikhonov regularization [34] in which original cost functional (6) is replaced with a regularized expression of the form

$$\mathcal{J}_\lambda(k) \triangleq \mathcal{J}(k) + \frac{\lambda}{2}\|k - \overline{k}\|^2_{\mathcal{Y}(I)}, \tag{31}$$

where $\lambda \in \mathbb{R}^+$ is an adjustable regularization parameter, $\overline{k}(T)$ represents a constitutive relation which our reconstruction $k(T)$ should not differ too much from, whereas $\|\cdot\|_{\mathcal{Y}(\mathcal{I})}$ is the Hilbert space norm in which we measure the deviation $(k-\overline{k})$. Thus, the regularization term in (31), i.e., the second one on the RHS, involves some additional information which needs to be specified a priori, namely, the choice of the reference constitutive relation $\overline{k}(T)$ and the space $\mathcal{Y}(\mathcal{I})$. As regards the reference function $\overline{k}(T)$, one natural possibility is to consider a constant value corresponding to a linearized version of constitutive relation (1). As regards the choice of the space $\mathcal{Y}(\mathcal{I})$, we will consider the following two possibilities:

(1) $\mathcal{Y}(I) = L_2(\mathcal{I})$, so that the regularization term in (31) becomes ($\lambda = \lambda_1$)

$$\frac{\lambda_1}{2}\|k - \overline{k}\|^2_{L_2(I)} = \frac{\lambda_1}{2}\int_{T_\alpha}^{T_\beta}(k - \overline{k})^2 ds \tag{32}$$

yielding the following L_2 gradient of the regularized cost functional

$$\boldsymbol{\nabla}_k^{L_2}\mathcal{J}_{\lambda_1}(s) = \int_\Omega \chi_{[T_\alpha, T(\mathbf{x})]}(s)\Delta T^* \, d\mathbf{x} - \int_{\partial\Omega}\chi_{[T_\alpha, T(\mathbf{x})]}(s)\frac{\partial T^*}{\partial n}\, d\sigma + \lambda_1(k - \overline{k}), \tag{33}$$

(2) $\mathcal{Y}(I) = \dot{H}^1(\mathcal{I})$, where $\dot{H}^1(\mathcal{I})$ denotes the Sobolev space equipped with the semi–norm $\|z\|_{\dot{H}^1(\mathcal{I})} \triangleq \int_{T_\alpha}^{T_\beta}\left(\frac{\partial z}{\partial s}\right)^2 ds$, $\forall_{z\in H^1(\mathcal{I})}$; the regularization term in (31) becomes ($\lambda = \lambda_2$)

$$\frac{\lambda_2}{2}\|k - \overline{k}\|^2_{\dot{H}^1(I)} = \frac{\lambda_2}{2}\int_{T_\alpha}^{T_\beta}\left(\frac{dk}{ds} - \frac{d\bar{k}}{ds}\right)^2 ds \tag{34}$$

yielding the following L_2 gradient of the regularized cost functional

$$\boldsymbol{\nabla}_k^{L_2}\mathcal{J}_{\lambda_2}(s) = \int_\Omega \chi_{[T_\alpha, T(\mathbf{x})]}(s)\Delta T^* \, d\mathbf{x} - \int_{\partial\Omega}\chi_{[T_\alpha, T(\mathbf{x})]}(s)\frac{\partial T^*}{\partial n}\, d\sigma - \lambda_2\frac{d^2k}{ds^2}|_{s\in[T_\alpha, T_\beta]}; \tag{35}$$

we remark that in obtaining (35) integration by parts was applied to the directional derivative of the regularization term together with boundary conditions (29b).

Expressions (33) and (35) can now be used to obtain suitable Sobolev gradients as discussed in Section 3. Computational tests illustrating the performance of the two forms of the Tikhonov regularization on a problem with noisy data will be presented in Section 6.3. In that Section we will also analyze the effect of the regularization parameters λ_1 and λ_2. We add that the stability and convergence of Tikhonov regularization using the Sobolev norm H^1 in the regularization term and applied to a very similar inverse problem was established rigorously in [14].

5 Shifting the Identifiability Interval

In Section 3 it was argued that the sensitivity of the cost functional $\mathcal{J}$ is essentially available on the identifiability interval $\mathcal{I}$ only, cf. Figure 1. The cost functional gradient may be formally extended outside this interval using the techniques described at the end of Section 3, however, these techniques merely ensure that the gradient is defined on the desired interval $\mathcal{L}$ and as such do not generate any new sensitivity information. Since, as demonstrated by our computational results reported in Section 6, such techniques are not capable of accurately reconstructing the relation $k(T)$ on an interval larger than the identifiability region, in the present Section we propose an approach to "shift" the identifiability region, so that the relation $k(T)$ can be reconstructed on a larger interval. In the limit, after performing several such shifts, the constitutive relation $k(T)$ can be reconstructed on the entire interval $\mathcal{L}$ which is of interest in a given problem. The idea behind shifting the identifiability region is to modify the data, such as the RHS source term and the boundary conditions, in problem (3), so that the solution of the modified problem spans a shifted interval $\mathcal{I}_{(1)} = [T_\alpha + h, T_\beta + h]$, where $h \in \mathbb{R}$. Hereafter we

will adhere to the convention that the indices enumerating shifts of the identifiability interval will appear as subscripts. This will allow us to distinguish them from the indices enumerating iterations in the solution of the optimization problem on a given identifiability region, cf. (9), which appear as superscripts. If the index representing the shifts of the identifiability region is skipped, the interval $\mathcal{I}_{(0)}$ is implied. Our approach is motivated by the following experimental procedure designed to reconstruct the constitutive relation $k(T)$ on an interval $\mathcal{L}$ larger than an individual identifiability interval.

Algorithm 1

- apply the heat sources $g_{(0)}(\mathbf{x}) = g(\mathbf{x})$ and the boundary conditions $T_{0,(0)} = T_0$ to the actual experimental system and obtain the measurements $\tilde{T}_{(0)}(\mathbf{x})$, $\mathbf{x} \in \Sigma$; use these measurements to reconstruct $k(T)$ on the identifiability region $\mathcal{I}_{(0)} = \mathcal{I}$ using relations (9), (21), (29) and (30)
- set $j = 0$

repeat

- set $j = j + 1$
- determine new heat source distribution $g_{(j)}(\mathbf{x})$ and boundary conditions $T_{0,(j)}$
- apply the new heat source distribution and boundary conditions to the experimental system and obtain new measurements $\tilde{T}_{(j)}(\mathbf{x})$, $\mathbf{x} \in \Sigma$
- use the new measurements $\tilde{T}_{(j)}(\mathbf{x})$, $\mathbf{x} \in \Sigma$ to reconstruct $k(T)$ on a new identifiability interval $\mathcal{I}_{(j)}$ using (9), (21), (29) and (30)

until $\bigcup_{p=1}^{j} \mathcal{I}_{(p)} \supset \mathcal{L}$, i.e., until the union of all shifted identifiability regions $\mathcal{I}_{(0)}, \ldots, \mathcal{I}_{(j)}$ covers the interval $\mathcal{L}$ where we seek to reconstruct the constitutive relation

This sequence of steps is illustrated schematically in Figure 2. While all other elements of Algorithm 1 should be obvious, the goal of the present Section is to show how to choose the RHS source term $g_{(j)}(\mathbf{x})$ and the boundary condition $T_{0,(j)}$, so that the identifiability interval $\mathcal{I}_{(j)}$ will be approximately shifted by a prescribed value h. Let us suppose that $T_{(0)}$ is a known solution of problem (3) spanning the identifiability interval $\mathcal{I}_{(0)}$ which we now want to shift by $h > 0$. We thus obtain

$$-\boldsymbol{\nabla} \cdot \Big[k(T_{(0)} + h)\, \boldsymbol{\nabla}(T_{(0)} + h)\Big] = \; g_{(1)} \qquad \text{in } \Omega, \tag{36a}$$

$$T_{0,(0)} + h = T_{0,(1)} \qquad \text{on } \partial\Omega, \tag{36b}$$

which can be regarded as equations defining the new source distribution $g_{(1)}$ and new boundary condition $T_{0,(1)}$ required for this shift. Since the function $g_{(1)}$ depends on the magnitude h of the shift, for small values $|h| \ll 1$ we can bypass this inconvenience using the Taylor series expansion

$$k(T_{(0)}(\mathbf{x}) + h) = k\,\Big(T_{(0)}(\mathbf{x})\Big) + h\,\frac{dk}{dT}\,\Big(T_{(0)}(\mathbf{x})\Big) + \mathcal{O}(h^2) \tag{37}$$

which holds for all $\mathbf{x} \in \Omega$, so that (36a) becomes

$$-\boldsymbol{\nabla} \cdot \Big[k\,\Big(T_{(0)}\Big)\,\boldsymbol{\nabla} T_{(0)}\Big] - h\boldsymbol{\nabla} \cdot \left[\frac{dk}{dT}\,\Big(T_{(0)}\Big)\,\boldsymbol{\nabla} T_{(0)}\right] = g_{(1)} + \mathcal{O}(h^2). \tag{38}$$

Thus, the source distribution corresponding to the shifted identifiability region $\mathcal{I}_{(1)}$ can be approximated to the leading order as

$$g_{(1)}(\mathbf{x}) \approx g_{(0)}(\mathbf{x}) - h\Delta\left[k\,\left(T_{(0)}(\mathbf{x})\right)\right], \tag{39}$$

where $g_{(0)}(\mathbf{x})$ is the source distribution corresponding to the original ("unshifted") identifiability interval. Expression (39) can be used in Algorithm 1 employing the most up–to–date estimate of the relation $k(T)$ resulting in

$$g_{(j+1)}(\mathbf{x}) \approx g_{(j)}(\mathbf{x}) - h\Delta\left[k_{(j)}\,\left(T_{(j)}(\mathbf{x})\right)\right]. \tag{40}$$

We note that in general the distance h may be allowed to vary from one shift to another. Shifting the identifiability interval has the effect of generating the sensitivity information over a different range of the state variable T. This might potentially have a detrimental effect on the reconstruction of $k(T)$ obtained on "earlier" identifiability intervals. In order for the reconstructions carried out on shifted intervals $\mathcal{I}_{(j)}$, $j \geq 1$, not to destroy the earlier reconstructions on $\mathcal{I}_{(0)}, \ldots, \mathcal{I}_{(j-1)}$, optimization on shifted intervals will be performed using a cost functional augmented with a Tikhonov–type penalty term, namely,

$$\mathcal{J}_{(j)}(k) \triangleq \mathcal{J}(k) + \frac{\gamma}{2}\int_{T_{\alpha,(0)}}^{T_{\beta,(j-1)}-\delta}[k(s) - k_{(j-1)}(s)]^2 ds, \tag{41}$$

where $\mathcal{J}(k)$ is defined in (6) and $\gamma, \delta \in \mathbb{R}^+$ are parameters. The purpose of including this additional term is to ensure that the reconstruction performed on the new (shifted) identifiability interval $\mathcal{I}_{(j)}$ preserves the estimate already constructed on the union of the previous intervals $\mathcal{I}_{(0)}, \ldots, \mathcal{I}_{(j-1)}$. It will also have the additional effect of regularizing the reconstruction procedure against measurement noise (cf. Section 4). We remark that if all the measurements $\{\tilde{T}_{(j)}\}_{j=1}^{P}$ were available from the beginning, then at least in principle one could consider an alternative approach based on solution of a single optimization problem on the union $\bigcup_{j=1}^{P}\mathcal{I}_j$ of all identifiability intervals. However, the difficulty with such an approach is that there would not be unique heat sources and boundary conditions defined on the composite identifiability interval. The methodology proposed in this Section is in our opinion well suited for an actual experimental procedure, as the experimental conditions (represented by the heat sources $g_{(j)}(\mathbf{x})$ and boundary conditions $T_{0,(j)}$) are adjusted in an *adaptive* fashion devised to produce temperature measurements in a desired identifiability region. Computational results illustrating Algorithm 1 combined with update formula (40) and augmented functional (41) will be presented in Section 6.4.

6 Computational Results

In this Section we describe the computational results obtained with our proposed method. Following a brief description of the numerical approaches used to solve the governing and the adjoint problem, we present some diagnostic tests concerning computation of the gradient at a given iteration. Next, we present the solution of the parameter estimation problem on a single identifiability interval with and without noise. Finally, we discuss the solution of a sequence

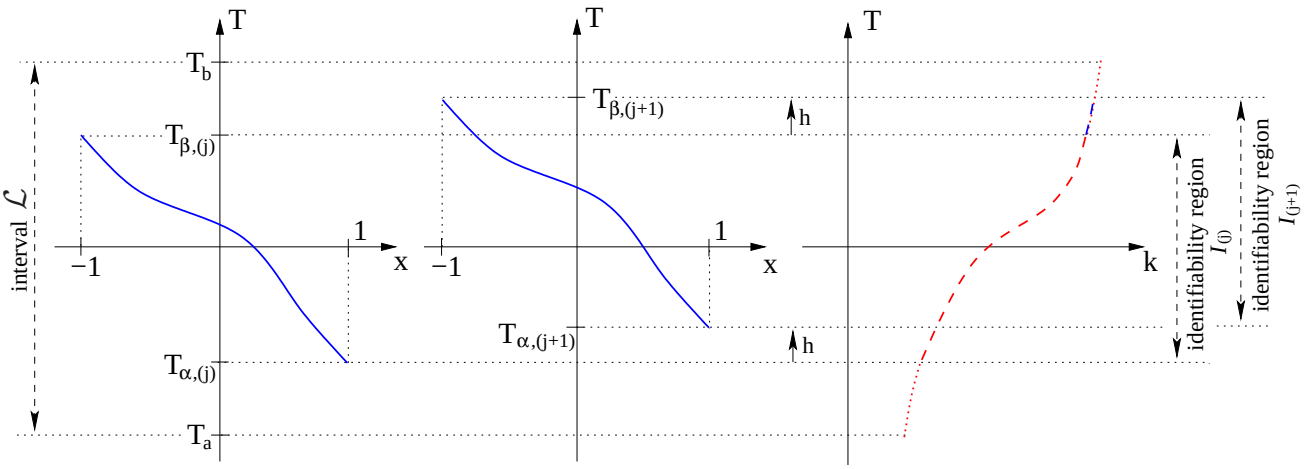

Fig. 2. Schematic illustrating the procedure for shifting the identifiability region. Notation is the same as in Figure 1. The left and middle graphs correspond to reconstructions performed at two consecutive intervals $\mathcal{I}_{(j)}$ and $\mathcal{I}_{(j+1)}$.

of parameter estimation problems on a set of identifiability regions shifted with respect to each other using the algorithm described in Section 5. For the sake of simplicity, our sample computations will be performed for a one–dimensional (1D) version of problem (3) with $\Omega = (-1, 1)$.

Governing system (3) and adjoint system (14) are discretized on a uniform grid with $N_x = 100$ grid points using the second–order central differences combined with the cubic spline interpolation of the function $k(T(x))$. For the purpose of this interpolation the interval $\mathcal{L}$ is discretized using an equispaced grid with $N_T = 200$ points, unless stated otherwise. The actual constitutive relation we seek to reconstruct is given by the function

$$\tilde{k}(T) = \arctan(T - 2.5) + b, \quad b = 2, \tag{42}$$

whose locally steep slope makes it representative of a range of constitutive relations typically encountered in thermodynamic systems. In parallel with discretization of the governing PDE, we also discretize the continuous measurements using pointwise measurement data which is typically available in actual experiments. We will assume that such pointwise measurements, denoted $\{\tilde{T}_i\}_{i=1}^M$, are available at a set of measurement points $\{\mathbf{x}_i\}_{i=1}^M$. We will in addition assume that the sensing domain can be regarded as a union $\Sigma = \bigcup_{i=1}^M \Sigma_i$ of disjoint subdomains $\Sigma_i \ni \mathbf{x}_i$, $i = 1, \ldots, M$, whose sizes $|\Sigma_i|$ are of the order of the grid size $\Delta x = \frac{2}{N_x - 1}$, so that $\int_{\Sigma_i} [\tilde{T}(\mathbf{x}) - T(\mathbf{x})]^2 \, d\mathbf{x} \approx [\tilde{T}(\mathbf{x}) - T(\mathbf{x})]^2 \, |\Sigma_i|$, $i = 1, \ldots, M$ (see Figure 3). In the computational tests reported below we used $M = 10$ (tests performed with different values of M yielded qualitatively similar results). To mimic an actual experimental procedure, on each identifiability interval $\mathcal{I}_{(j)}$, $j > 0$, relation (42) is used in combination with governing system (3) to obtain pointwise measurements $\{\tilde{T}_{i,(j)}\}_{i=1}^M$. Relation (42) is then "forgotten" and is reconstructed using gradient–based algorithm (9) on a single (Section 6.2), or several identifiability intervals (Section 6.4). While in the calculations validating our basic formulation (presented in Sections 6.1, 6.2 and 6.4) no noise was present in the measurements, its effect is addressed systematically in Section 6.3. In terms of the initial guess on the first identifiability region $\mathcal{I}_{(0)}$ we take a constant approximation k_0 to (42), whereas for the reconstruction problems on the shifted identifiability regions $\mathcal{I}_{(j)}$

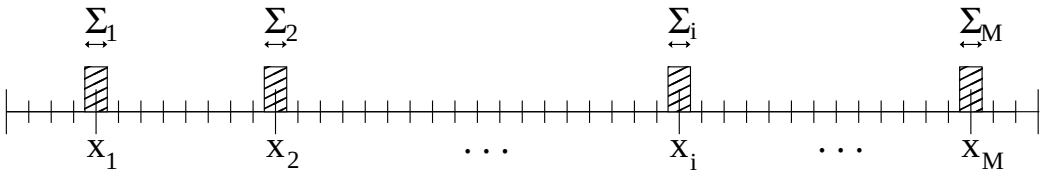

Fig. 3. Schematic showing discretization of continuous measurements $\tilde{T}(\mathbf{x})$, $\mathbf{x} \in \Sigma$ with pointwise measurements available at the discrete points $\mathbf{x}_1, \ldots, \mathbf{x}_M$. Hatched areas represent the individual sensing domains Σ_i, $i = 1, \ldots, M$.

we take $\hat{k}_{(j-1)}(T)$, i.e., the approximation of the constitutive relation obtained with the data on the interval $\mathcal{I}_{(j-1)}$. The initial distribution of the heat sources was $g_{(0)} = -\frac{(e^x-2x)^2}{1+(e^x-x^2-0.5)^2} - [\arctan(e^x - x^2 - 0.5) + 2]\,(e^x - 2)$ resulting in the identifiability region $\mathcal{I}_{(0)} = [1.3679, 3.7183]$. The interval over which we seek to reconstruct the constitutive relation is $\mathcal{L} = [0, 5.0862]$.

6.1 Validation of Gradients

In this Section we present results demonstrating the consistency of the cost functional gradients obtained with the approach described in Section 3. In Figure 4 we present the L_2 and several Sobolev H^1 gradients obtained at the first iteration. In the first place, we observe that as discussed in Section 3 the L_2 gradients do indeed exhibit discontinuities which makes them unsuitable for the reconstruction of constitutive relations with required properties, cf. (4). On the other hand, the gradients extracted in the Sobolev space H^1 are characterized by the required smoothness and therefore hereafter we will solely use the Sobolev gradients. We also observe that the two techniques for extending the gradients discussed in Section 3 [equations (28) and (29)–(30)] result in quite different behavior of the Sobolev gradients outside the identifiability region $\mathcal{I}$. These different behaviors will result in different quality of reconstruction of the constitutive relation. Next, in Figure 5 we present the results of a diagnostic test commonly employed to verify the correctness of the cost functional gradient [35]. It consists in computing directional differential (12) in two different ways, namely, using a finite–difference approximation and using the adjoint field, and then examining the ratio of the two results

$$\kappa(\epsilon) \triangleq \frac{\epsilon^{-1}\left[\mathcal{J}(k + \epsilon k') - \mathcal{J}(k)\right]}{\int_{T_a}^{T_b} \boldsymbol{\nabla}_k \mathcal{J}(s)\, k'(s)\, ds} \tag{43}$$

for a range of values of ϵ. We emphasize that in view of Riesz identity (12) it does not matter which inner product (i.e., L_2 vs. H^1) is adopted in the expression in the numerator in (43). If the gradient $\boldsymbol{\nabla}_k \mathcal{J}(k)$ is computed correctly, then for intermediate values of ϵ, $\kappa(\epsilon)$ should be close to the unity. Remarkably, this behavior can be observed in Figure 5 over a range of ϵ spanning about 10 orders of magnitude for two different perturbations $k'(T)$. Furthermore, we also emphasize that refining the discretization of the interval $\mathcal{L}$ yields values of $\kappa(\epsilon)$ much closer to the unity. As can be expected, the quantity $\kappa(\epsilon)$ deviates from the unity for very small values of ϵ, which is due to the subtractive cancellation (round–off) errors, and also for large values of ϵ, which is due to the truncation errors.

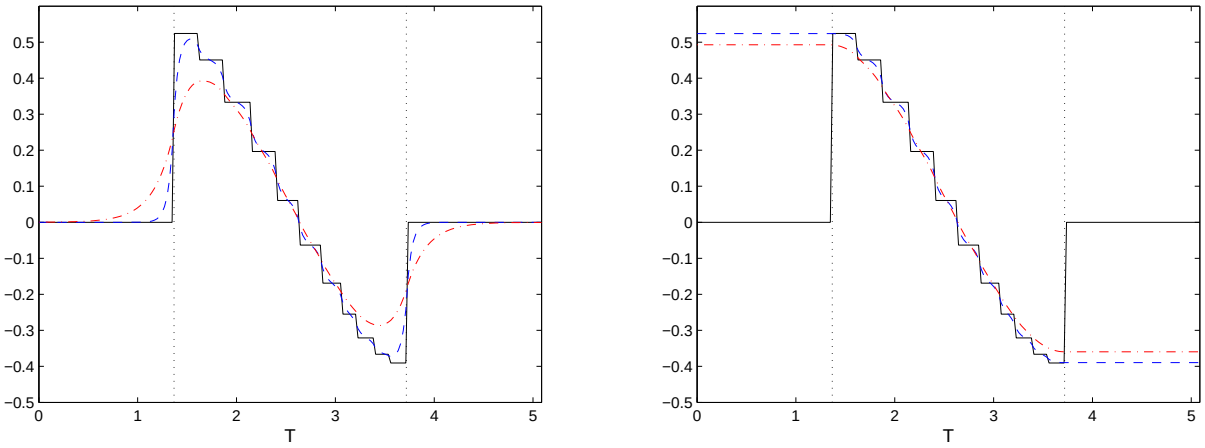

(a) (b)

Fig. 4. Comparison of (solid line) the L_2 gradient $\nabla^{L_2}\mathcal{J}$ and the Sobolev gradients $\nabla^{H^1}\mathcal{J}$ defined (a) in (28) and (b) in (29)–(30) for different values of the smoothing coefficient (dashed line) $l = 0.05$ and (dash–dotted line) $l = 0.2$ at the first iteration with the initial guess $k_0 = const = 2.13$. The vertical dotted lines represent the boundaries of the identifiability interval $\mathcal{I}_{(0)}$.

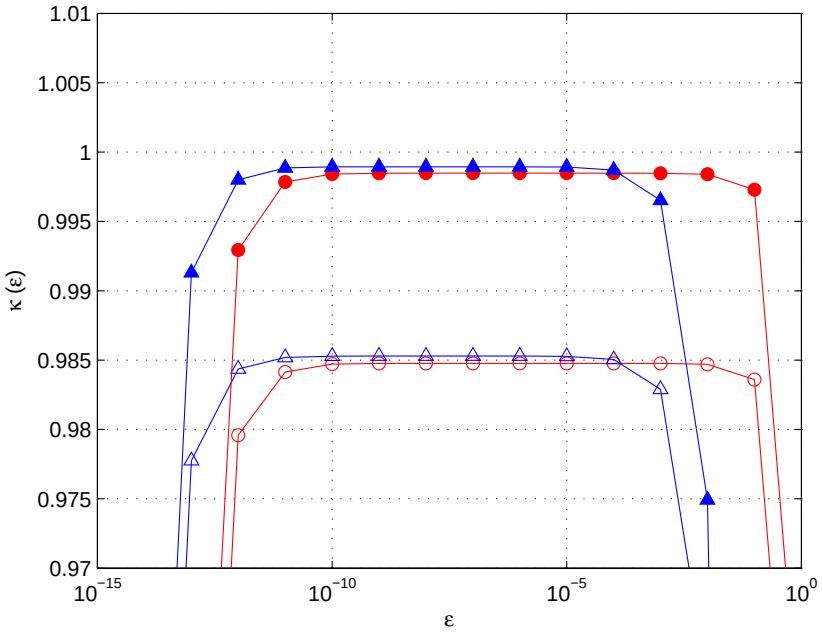

Fig. 5. The behavior of $\kappa(\epsilon)$ for different perturbations (circles) $k'(T) = \exp(-T^2/10)$ and (triangles) $k'(T) = -0.1T^2 + 10$ using different discretizations of the interval $\mathcal{L}$: (empty symbols) $N_T = 200$ and (filled symbols) $N_T = 2000$.

6.2 Reconstruction on a Single Identifiability Interval

We solve minimization problem (7) using the BFGS algorithm [26] and, unless indicated otherwise, Sobolev gradients computed with $l = 0.2$ which was found by trial–and–error to maximize

the rate of convergence of iterations (9). The termination condition used was $\left|\frac{\mathcal{J}(k^{(n)})-\mathcal{J}(k^{(n-1)})}{\mathcal{J}(k^{(n-1)})}\right| < 10^{-6}$. The behavior of the cost functional $\mathcal{J}(k^{(n)})$ as a function of the iteration count n is shown in Figure 6a for the Sobolev gradients defined in (28) and in (29)–(30). We note that while in both cases a decrease over several orders of magnitude is observed in just a few iterations, in the first case the cost functional eventually drops to very small values. The effect of the different values of the constant initial guess k_0 on the decrease of the cost functional is illustrated in Figure 6b. We note that the cost functional $\mathcal{J}(k^{(n)})$ decreases rapidly for all investigated values of the constant k_0, although the iterations saturate at different levels. It is interesting to observe that the best results were obtained for the initial guess $k_0 = \frac{1}{M}\sum_{i=1}^{M}\tilde{k}(\tilde{T}_i) = 2.1499$ which is the algebraic mean of the values of the true constitutive relation $\tilde{k}(T)$ evaluated at the "measured" temperatures. Reconstructions $\hat{k}(T)$ of the constitutive relation obtained using the Sobolev gradients defined in (28) and in (29)–(30) are shown in Figures 7 and 8, respectively. We note that while the quality of the reconstruction on the identifiability region $\mathcal{I}$ is comparable in the two cases, outside the identifiability region the second approach clearly offers superior accuracy. In Figure 9 we show the reconstructions $\hat{k}(T)$ of the constitutive relation obtained for different values of the constant initial guess k_0 (the same values as used in Figure 6b). We conclude that, since the reconstructed relations are quite different, the iterations starting from different initial guesses converge in fact to different local minimizers. However, these differences notwithstanding, all reconstructions shown in Figure 9 capture the main features of the true constitutive relation (42). We also emphasize that there is a range of values of the initial guess k_0 for which the quality of reconstruction is excellent (cf. Figure 8 and 9d). Next, in Figure 10a we show the solutions $T(x;k)$ to problem (3) corresponding to the reconstructed conductivity $\hat{k}(T)$, cf. Figure 8, and the true conductivity $\tilde{k}(T)$, cf. (42), together with the measurements $\{\tilde{T}_i\}_{i=1}^{10}$ used as data in the solution of the problem. We note excellent agreement of the solutions obtained based on the reconstructed and measured constitutive relations. Since the solutions $T(x)$ corresponding to the reconstructed and true constitutive relations cannot be distinguished in Figure 10a, in Figure 10b we show the error $|T(x;\hat{k}) - T(x;\tilde{k})|$ corresponding to the reconstruction $\hat{k}$ obtained using the two definitions of the Sobolev gradients given in Section 3. Finally, we remark that, although the Sobolev gradients defined in (28) resulted in a larger decrease of the cost functional in Figure 6a and smaller errors evident in Figure 10b, this is in fact offset by the more favorable behavior of the Sobolev gradients defined in (29)–(30) outside the identifiability region. Thus, this second approach will be used in the sequel to perform reconstruction on shifted identifiability regions.

6.3 Reconstruction in the Presence of Noise

In this Section we first assess the effect of noise on the reconstruction without Tikhonov regularization and then study the efficiency of the regularization techniques introduced in Section 4. In Figure 11 we revisit the case presented first in Figure 8, now for measurements contaminated with 1%, 3%, 5% and 10% uniformly distributed noise and without Tikhonov regularization. As expected, we see that increasing levels of noise lead to oscillatory instabilities developing in the reconstructed constitutive relations $k(T)$. We further observe that this instability is somewhat less pronounced in reconstructions performed with "smoother" gradients [i.e., corresponding to

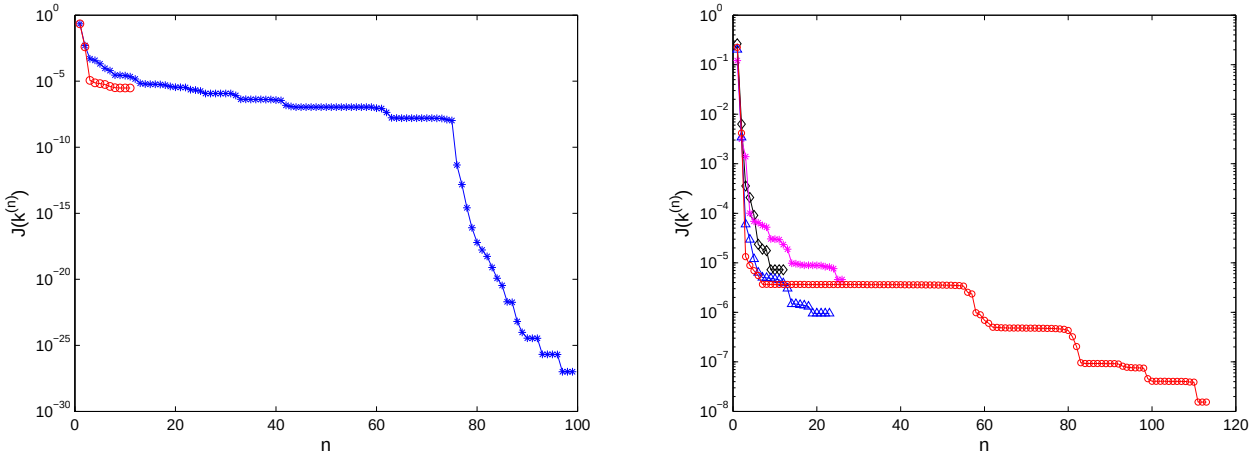

(a) (b)

Fig. 6. (a) Decrease of the cost functional $\mathcal{J}(k^{(n)})$ with iterations n using the Sobolev gradient $\boldsymbol{\nabla}^{H^1}\mathcal{J}$ defined (asterisks) in (28) and (circles) in (29)–(30) with $l = 0.2$; the initial guess was $k_0 = 2.13$, (b) decrease of the cost functional $\mathcal{J}(k^{(n)})$ with iterations n for different initial guesses: (diamonds) $k_0 = 2.5$, (asterisks) $k_0 = 1.5$, (triangles) $k_0 = 2$, and (circles) $k_0 = \dfrac{1}{M}\sum_{i=1}^{M}\tilde{k}(\tilde{T}_i) = 2.1499$ obtained with the Sobolev gradients defined in (29)–(30).

larger values of the length–scale parameter ℓ in (29a)]. This regularizing effect of the Sobolev gradients was already discussed in [32].

The effect of the Tikhonov regularization is studied in Figure 12 where we illustrate the performance of the two techniques described in Section 4, cf. (32) and (34), on the reconstruction problem with 10% noise in the measurement data (i.e., the "extreme" case presented in Figure 11). We conclude that regularization with the Sobolev $\dot{H}^1(\mathcal{I})$ term tends to give somewhat better results than regularization with the L_2 term, cf. Figures 12(a,b) and 12(c,d). In both cases, with increasing values of the regularization parameters λ_1 and λ_2 the reconstructed constitutive relations become smoother at the price however of larger reconstruction errors which is a well–known trade–off involved in Tikhonov regularization. Systematic methods for determining optimal values of regularization parameters are discussed for instance in [34]. Finally, in Figure 13 we present the relative reconstruction errors $\|\hat{k} - \tilde{k}\|_{L_1(\mathcal{I})} \,/\, \|\tilde{k}\|_{L_1(\mathcal{I})}$ obtained using the approaches discussed in Section 4 for data with different noise levels and averaged over 100 noise samples. We note that on the whole regularization with the Sobolev $\dot{H}^1(\mathcal{I})$ term performs slightly better than regularization with the $L_2(\mathcal{I})$ term. Reconstructions employing the Sobolev gradients alone with no Tikhonov regularization produce significantly poorer results especially for larger noise amplitudes. We close this Section by concluding that Tikhonov regularization performs as expected in problems with significant noise levels in the measurement data.

6.4 Reconstruction on Shifted Identifiability Intervals

In this Section we implement the approach for shifting the identifiability region described in Section 5. We reiterate that the goal is to extend the range of the state variable T on which

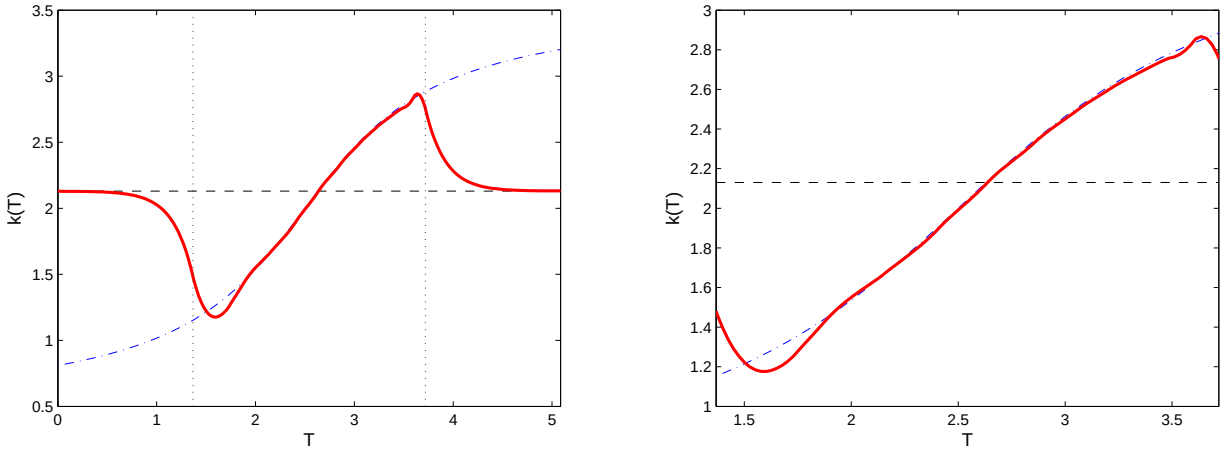

(a) (b)

Fig. 7. Reconstruction $\hat{k}(T)$ of the constitutive relation obtained using the Sobolev gradients defined in (28) on (a) the interval $\mathcal{L}$ and (b) close–up view showing the identifiability interval $\mathcal{I}_{(0)}$. The dash–dotted line represents the true constitutive relation (42), the solid line is the reconstruction, whereas the dashed line represents the initial guess $k_0 = 2.13$; the vertical dotted lines in the figure on the left represent the boundaries of the identifiability interval $\mathcal{I}_{(0)}$.

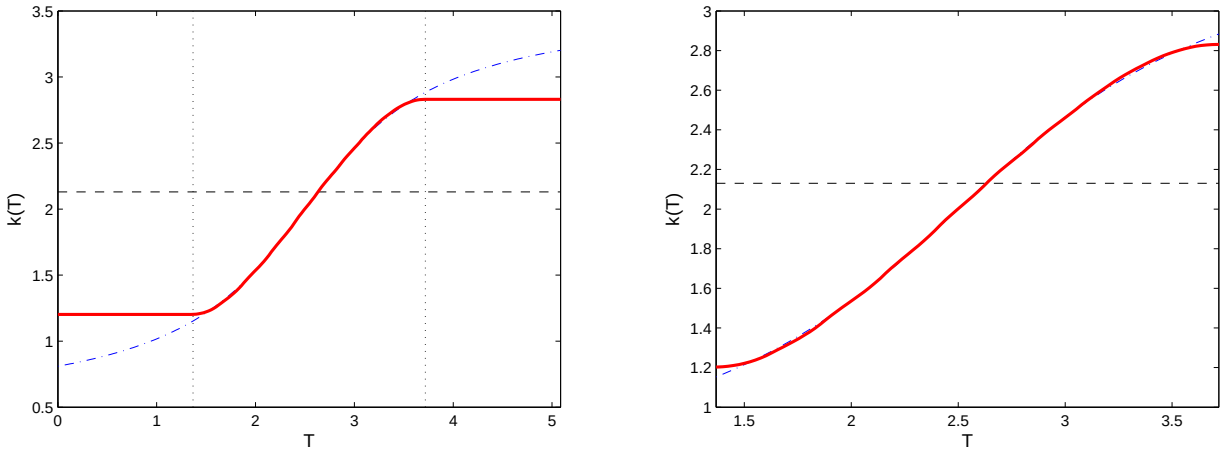

(a) (b)

Fig. 8. Reconstruction $\hat{k}(T)$ of the constitutive relation obtained using the Sobolev gradients defined in (29)–(30) on (a) the interval $\mathcal{L}$ and (b) close–up view showing the identifiability interval $\mathcal{I}_{(0)}$. The dash–dotted line represents the true constitutive relation (42), the solid line is the reconstruction, whereas the dashed line represents the initial guess $k_0 = 2.13$; the vertical dotted lines in the figure on the left represent the boundaries of the identifiability interval $\mathcal{I}_{(0)}$.

one can accurately reconstruct the constitutive relation so as to cover the entire interval $\mathcal{L}$. As implied by Algorithm 1, we do this by solving a sequence of reconstruction problems, each with the cost functional, the RHS source term and boundary conditions in governing equation (3) chosen as described in Section 5. From the practical point of view, this mimics performing a sequence of laboratory experiments, each in suitably chosen conditions represented by $g_{(j)}$ and $T_{0,(j)}$, to generate the data for the reconstruction process on different identifiability intervals.

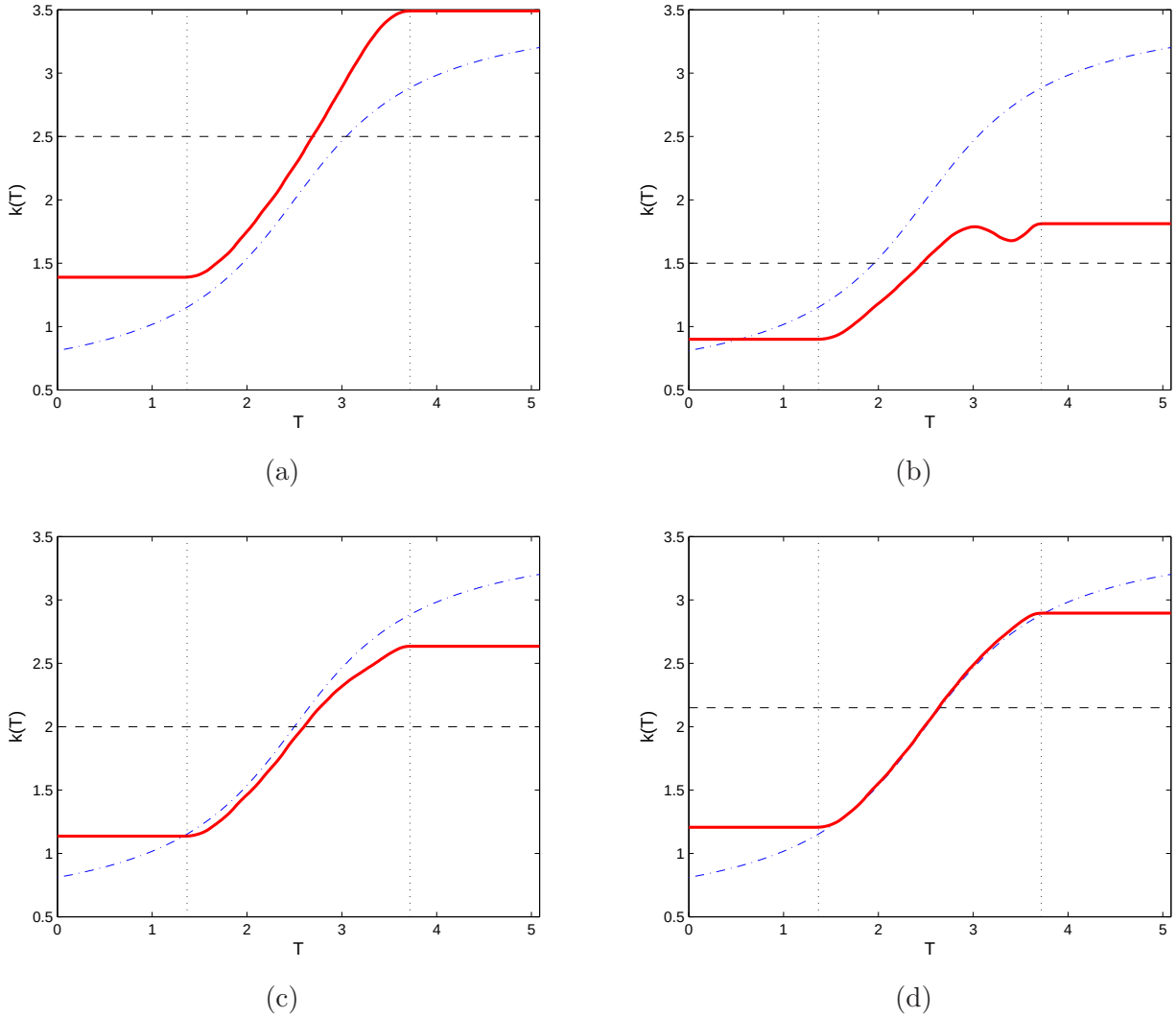

Fig. 9. Reconstruction $\hat{k}(T)$ of the constitutive relation obtained using different initial guesses (a) $k_0 = 2.5$, (b) $k_0 = 1.5$, (c) $k_0 = 2$ and (d) $k_0 = \frac{1}{M}\sum_{i=1}^{M} \tilde{k}(\tilde{T}_i) = 2.1499$, and the Sobolev gradients defined in (29)–(30). The dash–dotted lines represent the true constitutive relation (42), the solid lines are the reconstructions, whereas the dashed lines represent initial guesses; the vertical dotted lines represent the boundaries of the identifiability interval $\mathcal{I}_{(0)}$.

Results obtained with this approach and performing shifts in one direction only, i.e., towards larger values of T, are shown in Figures 14 and 15 for $P = 12$ and $P = 50$ shifts, respectively. The shifts were performed assuming $h = 0.1$ in (40) and $\gamma = 12$ in (41). The parameter δ in (41) was equal to 6% and 3% of the width of the current identifiability interval respectively in the problems with 12 and 50 shifts. All of these parameters were chosen empirically to maximize the quality of the reconstruction. We observe that, as compared to the reconstruction performed on $\mathcal{I}_{(0)}$ only, now a good estimate of the constitutive relation $k(T)$ is obtained for a much broader range of T, although the quality of this reconstruction slowly degrades as the number of shifts is increased. Moreover, as is evident from Figures 8b, 14c, and 15c, this is achieved at the cost of a slight deterioration of the final reconstruction $\hat{k}_{(P)}(T)$ on the original identifiability interval $\mathcal{I}_{(0)}$ as compared to the reconstruction $\hat{k}_{(0)}(T)$ obtained without any shifts. Finally, in Figure

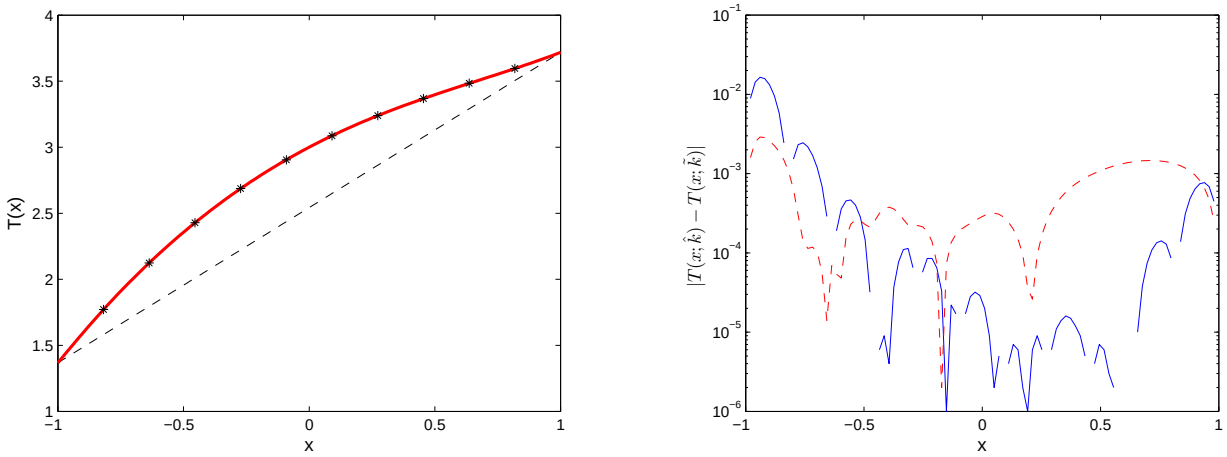

(a) (b)

Fig. 10. (a) Solution $T(x,k)$ of governing equation (3) corresponding to (solid line) the reconstructed constitutive relation $\hat{k}$, (dashed line) the initial guess $k_0 = 2.13$, and (dash–dotted line) the true constitutive relation $\tilde{k}$; asterisks represent the measurement data $\{\tilde{T}_i\}_{i=1}^{10}$, (b) the error $|T(x;\hat{k})-T(x;\tilde{k})|$ between the solution of governing equation (3) corresponding to $\hat{k}$ obtained using the Sobolev gradients defined (solid line) in (28) and (dashed line) in (29)–(30), and the solution corresponding to the true constitutive relation (42).

16 we present the reconstruction $\hat{k}_{(2P)}(T)$ of the constitutive relation obtained by shifting the identifiability region in both directions. This is achieved by performing the shifts towards larger and smaller values of T in an interchanging manner. The parameters used were $h = 0.1$, $\gamma = 8$ and $\delta = 4\% \times$ [width of the current identifiability region]. We observe that in this problem as well good reconstruction of the constitutive relation $k(T)$ was obtained on the entire interval $\mathcal{L}$.

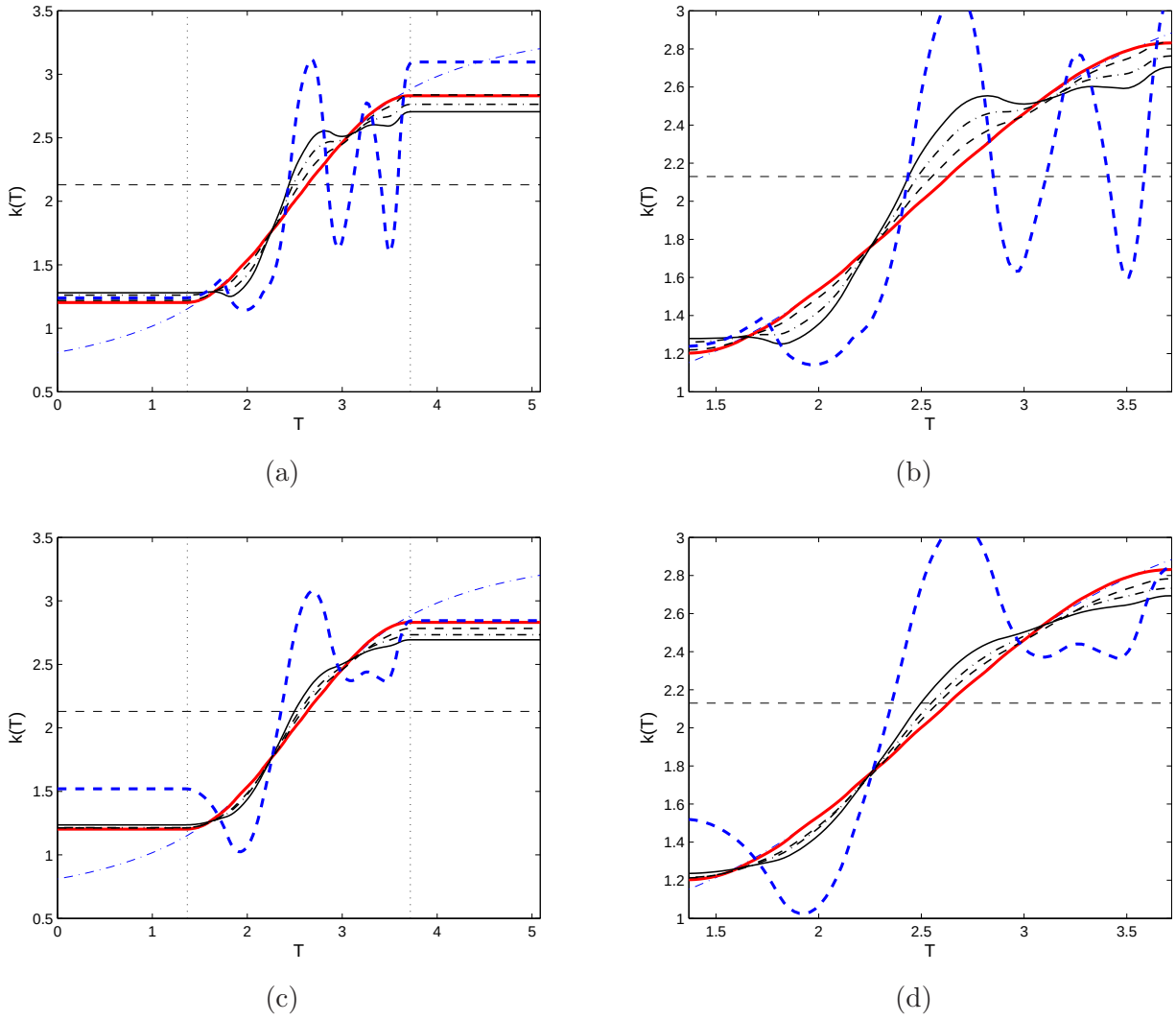

Fig. 11. Reconstruction $\hat{k}(T)$ of the constitutive relation obtained using the Sobolev gradients defined in (29)–(30) with (a,b) $\ell = 0.2$ and (c,d) $\ell = 0.4$ and different noise levels in the measurement data: (thick solid line) no noise, (dashed line) 1%, (dash–dotted line) 3%, (thin solid line) 5%, and (thick dashed line) 10%. The dashed horizontal line represents the initial guess $k_0 = 2.13$, whereas the vertical dotted lines in the figures on the left represent the boundaries of the identifiability interval $\mathcal{I}_{(0)}$. Figures (a) and (c) correspond to the interval $\mathcal{L}$, whereas figures (b) and (d) show a close–up view of the identifiability interval $\mathcal{I}_{(0)}$.

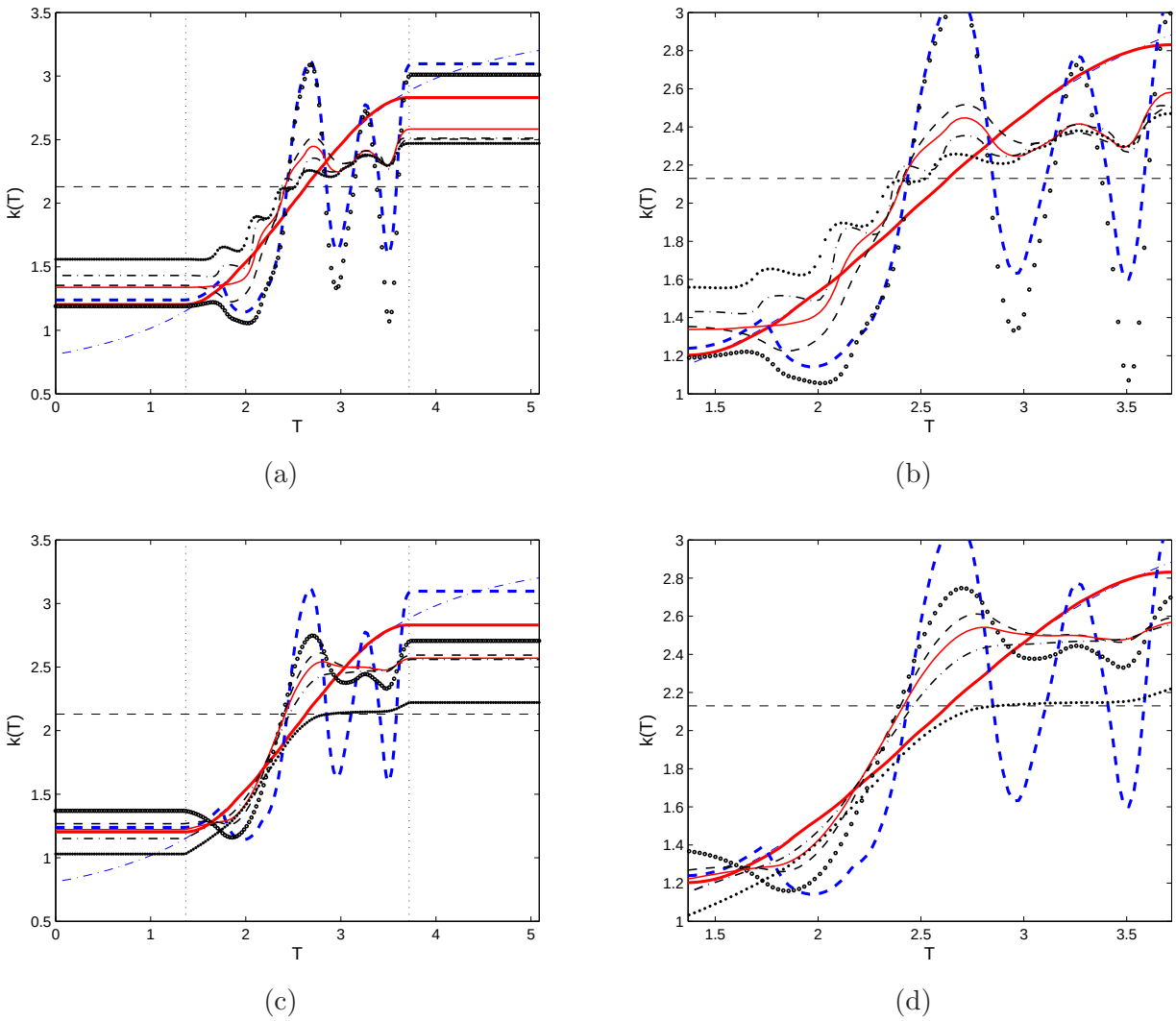

Fig. 12. Effect of Tikhonov regularization on the reconstruction from the measurement data with 10% noise using (a,b) regularization term (32) and (c,d) regularization term (34). In Figures (a) and (b) the following values of the regularization parameter were used: (thick dashed line) $\lambda_1 = 0$, (circles) $\lambda_1 = 0.01$, (dashed line) $\lambda_1 = 0.05$, (thin solid line) $\lambda_1 = 0.1$, (dash–dotted line) $\lambda_1 = 0.2$, and (dots) $\lambda_1 = 0.4$. In Figures (c) and (d) the following values of the regularization parameter were used: (thick dashed line) $\lambda_2 = 0$, (circles) $\lambda_2 = 0.001$, (dashed line) $\lambda_2 = 0.003$, (thin solid line) $\lambda_2 = 0.005$, (dash–dotted line) $\lambda_2 = 0.01$, and (dots) $\lambda_2 = 0.02$. The dashed horizontal line represents the initial guess $k_0 = 2.13$, whereas the vertical dotted lines in the figures on the left represent the boundaries of the identifiability interval $\mathcal{I}_{(0)}$. Figures (a) and (c) correspond to the interval $\mathcal{L}$, whereas figures (b) and (d) show a close–up view of the identifiability interval $\mathcal{I}_{(0)}$.

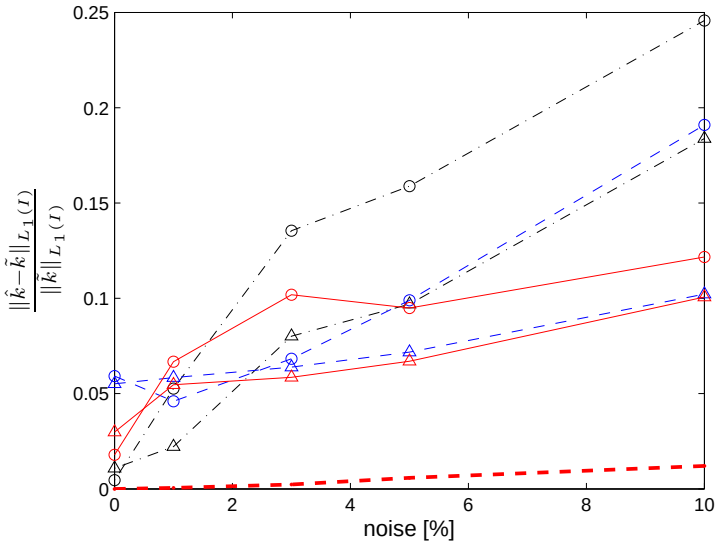

Fig. 13. Relative L_1 reconstruction errors $\|\hat{k}-\tilde{k}\|_{L_1(\mathcal{I})} \,/\, \|\tilde{k}\|_{L_1(\mathcal{I})}$ obtained in the presence of noise with the amplitude indicated and averaged over 100 samples: (dash–dotted line) reconstruction with Sobolev gradients and without Tikhonov regularization [(circles) $\ell = 0.2$, (triangles) $\ell = 0.4$], (dashed line) reconstruction with L_2 Tikhonov regularization term (32) [(circles) $\lambda_1 = 0.01$, (triangles) $\lambda_1 = 0.1$], and (solid line) reconstruction with $\dot{H}^1$ Tikhonov regularization term (34) [(circles) $\lambda_2 = 0.005$, (triangles) $\lambda_2 = 0.003$]. The thick dashed line represents the "error" in the exact constitutive relation (42) obtained by adding noise to T.

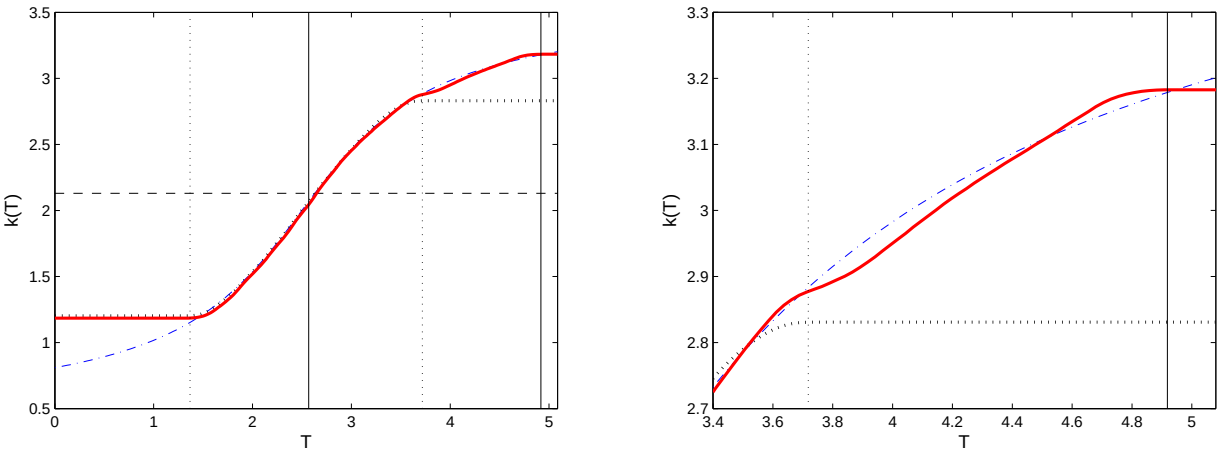

(a) (b)

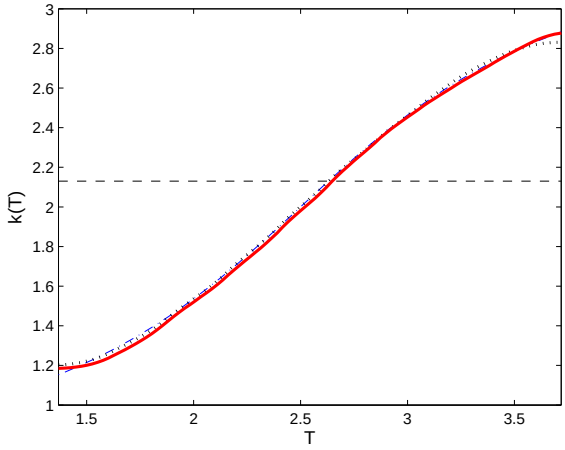

(c)

Fig. 14. Reconstruction $\hat{k}_{(P)}(T)$ of the constitutive relation on an union of $P = 12$ shifted identifiability regions: (a) the interval $\mathcal{L}$, (b) magnification of the region where the different identifiability intervals overlap, and (c) the initial identifiability interval $\mathcal{I}_{(0)}$. The dash–dotted line represents the true constitutive relation (42), the solid line is the reconstruction $\hat{k}_{(P)}(T)$ after $P = 12$ shifts, whereas the dotted line represents the reconstruction $\hat{k}_{(0)}(T)$ obtained without any shifts; the vertical lines represent the boundaries of (dotted) the interval $\mathcal{I}_{(0)}$ and (solid) the interval $\mathcal{I}_{(12)}$.

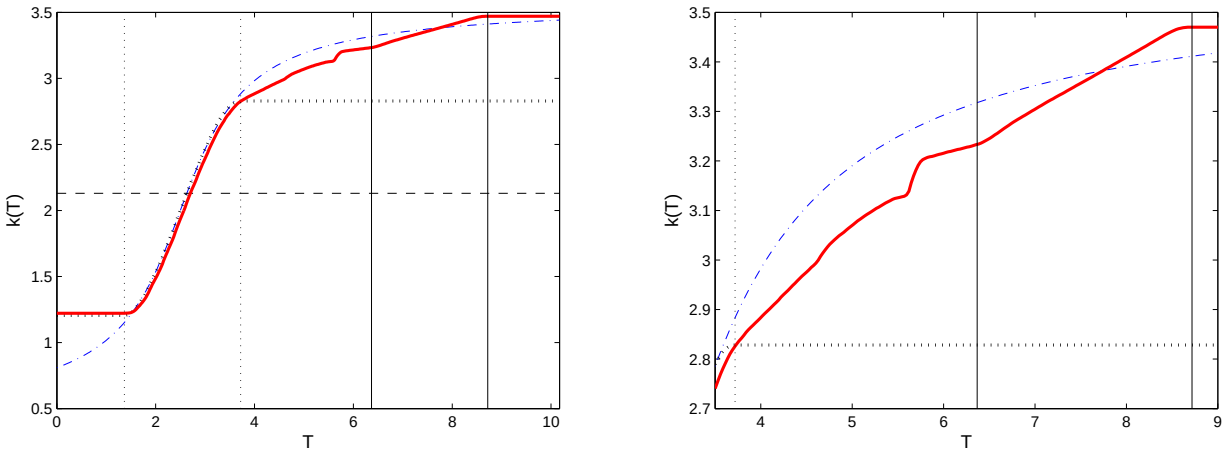

(a)

(b)

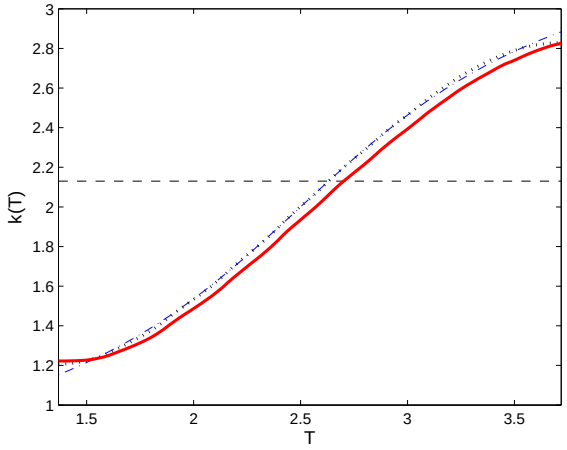

(c)

Fig. 15. Reconstruction $\hat{k}_{(P)}(T)$ of the constitutive relation on an union of $P = 50$ shifted identifiability regions: (a) the interval $\mathcal{L}$, (b) magnification of the region where the different identifiability intervals overlap, and (c) the initial identifiability interval $\mathcal{I}_{(0)}$. The dash–dotted line represents the true constitutive relation (42), the solid line is the reconstruction $\hat{k}_{(P)}(T)$ after $P = 50$ shifts, whereas the dotted line represents the reconstruction $\hat{k}_{(0)}(T)$ obtained without any shifts; the vertical lines represent the boundaries of (dotted) the interval $\mathcal{I}_{(0)}$ and (solid) the interval $\mathcal{I}_{(50)}$.

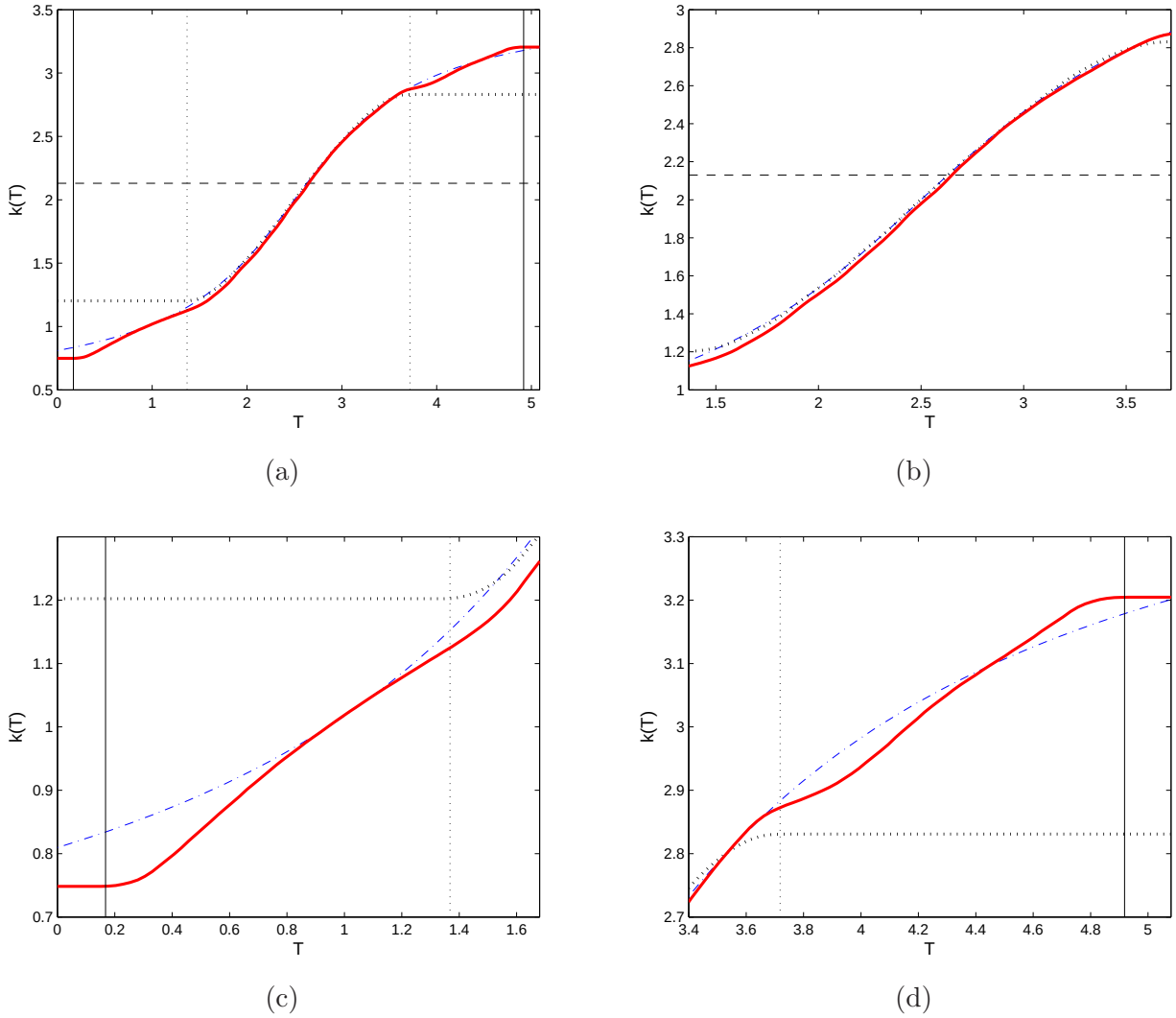

Fig. 16. Reconstruction $\hat{k}_{(2P)}(T)$ of the constitutive relation obtained with the original identifiability region shifted interchangeably towards larger and smaller values of T: (a) interval $\mathcal{L}$, (b) the initial identifiability interval $\mathcal{I}_{(0)}$, and (c,d) magnification of the regions where the different identifiability intervals overlap. The dash–dotted line represents the true constitutive relation (42), the solid line is the reconstruction $\hat{k}_{(2P)}(T)$ after $P = 12$ shifts in each direction, whereas the dotted line represents the reconstruction $\hat{k}_{(0)}(T)$ obtained without any shifts; the vertical lines represent the boundaries of (dotted) the interval $\mathcal{I}_{(0)}$ and (solid) the union $\cup_{j=0}^{2P}\mathcal{I}_{(j)}$.

7 Conclusions and Summary

In this study we investigated a novel computational approach to reconstruction of constitutive relations based on incomplete measurement data. This parameter estimation problem is solved using a gradient–based optimization technique in which the sensitivities of the cost functional with respect to the form of the constitutive relation are computed using a suitably–defined adjoint system. The main challenge inherent in this problem follows from the fact that the control variable is a function of the state, rather than the independent variable in the governing system. We studied the problem in the context of the "optimize–then–discretize" approach to PDE–constrained optimization and demonstrated how using the Kirchhoff transformation one can obtain an expression of the cost functional gradient more convenient from the computational point of view than derived in earlier studies [6]. We also argued that the traditional L_2 cost functional gradients are discontinuous and therefore unsuitable for reconstruction of smooth constitutive relations. It was shown that this difficulty can be resolved by using the Sobolev gradients defined consistently with the functional setting of the problem in the optimization algorithm. Finally, we proposed and validated a procedure allowing one to shift the identifiability region, and in this way reconstruct the constitutive relation over a much broader range of the state variable. A novel aspect of this approach is an adaptive adjustment of experimental parameters needed to produce measurements in a prescribed identifiability region. We add that this procedure also relies on the use of the Sobolev gradients. Computational tests demonstrated the feasibility of the proposed approach on a simple 1D model problem, and constitute a proof of concept for the method. These elements represent the key original contributions of this work. The results obtained underline the importance of a good choice of the initial guess k_0 for iterative procedure (9). Such an initial guess can be taken as a constant matched to reflect the bulk properties of the material. We also addressed the important issue of reconstruction in the presence of random noise in the measurement data, and showed that the classical Tikhonov regularization involving L_2 and H^1 regularization term is able to stabilize the reconstruction process, even for significant noise levels. Our computations indicate that the use of suitable Sobolev gradients in the reconstruction process may also have some regularizing effect. In addition to the results analyzed in detail in Section 6, we also tested the algorithm on several other problems involving different forms of the actual constitutive relation $\tilde{k}(T)$ and the RHS function g, and in all cases obtained good results. We note that, in particular, using the Sobolev gradients we were also able to obtain satisfactory results in situation in which $\boldsymbol{\nabla} T(\mathbf{x};\tilde{k}) \approx \mathbf{0}$ and $\Delta T(\mathbf{x};\tilde{k}) \approx 0$ at some points $\mathbf{x} \in \Omega$. We emphasize that such cases are especially challenging, since as is evident from the expanded form of (3a), in these situations the reconstruction problem might possibly also admit solutions $k(T)$ unbounded at $T = T(\mathbf{x})$.

Our future work will involve extensions of the present approach to more complicated problems involving systems of coupled PDEs depending on time and defined on domains with higher dimensions. It is particularly interesting to consider problems in which the constitutive relation appearing in one equation depends on the state variable governed by a different equation (e.g., reconstruction of the temperature dependence of the viscosity coefficient in the momentum equation where the temperature is governed by a separate energy equation). We are already investigating such problems and results will be reported in the near future. In the context of such systems another interesting issue is the reconstruction of anisotropic constitutive relations,

i.e., expressed by the tensorial version of (1). A still more challenging problem is related to reconstruction of constitutive relations in systems involving phase changes. In addition to the governing PDE in the form of a free–boundary problem, one would also have to deal with constitutive relations with distinct functional forms in each of the phases. When studying such more complicated problems, close attention will need to be paid to the problem of ensuring consistency of the reconstructed constitutive relation with the second principle of thermodynamics. In general, this can be done by revisiting the inequality–constrained version (10) of the problem with the constraint given in the form of the complete Clausius–Duhem inequality.

Acknowledgments

The authors wish to acknowledge generous funding provided for this research by the Natural Sciences and Engineering Research Council of Canada (Collaborative Research and Development Program), Ontario Centres of Excellence — Centre for Materials and Manufacturing, and General Motors of Canada. We are thankful to Prof. Dmitry Pelinovsky for helpful discussions.

A Minimum Principle for Problem (3)

Theorem A.1 *Let $T \in C^2(\Omega) \cap C^0(\overline{\Omega})$ be a solution of (3). If $k(T) > 0$, $\forall\, T \in \mathcal{I}$, and $g(\mathbf{x}) > 0$, $\forall \mathbf{x} \in \Omega$, then*

$$\min_{\mathbf{x}\in\overline{\Omega}} T(\mathbf{x}) = T_\alpha = \min_{\mathbf{x}\in\partial\Omega} T_0(\mathbf{x}),$$

i.e., the minimum is attained on the boundary $\partial\Omega$.

PROOF. Although Theorem A.1 may be obtained as a special case from a more general result given in [36], we present here the proof for the sake of completeness. We prove this theorem by contradiction. Let us assume that the minimum of the solution T is attained at an interior point $\tilde{\mathbf{x}} \in \Omega$. Since $\nabla T(\tilde{\mathbf{x}}) = 0$, Equation (3a) takes form $-k(T)\,\Delta T = g$ at the point $\tilde{\mathbf{x}}$. Therefore, by continuity, we would have $\Delta T < 0$ in a small neighborhood of $\tilde{\mathbf{x}}$ which would contradict the assumption that $T(\tilde{\mathbf{x}})$ is a minimum. □

B Differentiability of Map (5)

In this Appendix we outline the proof of a theorem concerning the differentiability of map (5) from the constitutive relations to measurements. In its main idea our proof is analogous to the proof presented in [6] for a different (time–dependent) problem, however, a number of intermediate estimates are different. We thus consider problem (3) in a general bounded domain Ω with a $C^{1,1}$ boundary and start by defining the following functional spaces for the dependent

variable T

$$\mathcal{T} = \{T \in H^1(\Omega); T = 0 \text{ on } \partial\Omega\}, \quad H = L_2(\Omega), \quad \mathcal{T}' = H^{-1}(\Omega), \tag{B.1}$$

where for simplicity we have assumed homogeneous Dirichlet data. The inner product $((\cdot,\cdot))_*$ in the dual space $\mathcal{T}'$ is defined as

$$((u,v))_* = (D^{-1}u, D^{-1}v)_{H^1}, \tag{B.2}$$

where $D = \Delta$ is the canonical isomorphism between $\mathcal{T}$ and $\mathcal{T}'$, i.e.,

$$\text{if } u \in \mathcal{T} \quad \Longrightarrow \quad D\,u = \Delta u \in \mathcal{T}'. \tag{B.3}$$

We consider two weak formulations of governing system (3), namely, a variational formulation in the space $\mathcal{T}$ defined as follows

$$\int_\Omega k(T)\,\nabla T \cdot \nabla u\,d\mathbf{x} = \int_\Omega g\,u\,d\mathbf{x}, \qquad T, u \in \mathcal{T}, \tag{B.4}$$

and a weaker one obtained from (B.4) by setting $u = D^{-1}w$

$$\int_\Omega V(T)\cdot w\,d\mathbf{x} = ((g,w))_*, \qquad \forall w \in H, \tag{B.5}$$

where $V(T)$ is defined in (15). Now, we state a differentiability result for the solution $T = T(\mathbf{x};k)$ of equation (B.4) in which the solution $T(\mathbf{x};k)$ is treated as an element of $L_2(\Omega)$, cf. (5) and (6).

Theorem B.1 *Assume that m_k, cf.* (4)*, is sufficiently large and solutions of* (3) *satisfy $\|\boldsymbol{\nabla} T\|_{L^\infty(\Omega)} < \infty$. Then the map $k \to T(\cdot;k)$ from $\mathcal{K}$ to $L_2(\Sigma)$ defined by* (B.4) *is Fréchet–differentiable in the norm $H^1(\mathcal{I})$.*

PROOF. Let k' denote the variation of k such that $k, \check{k} \triangleq k + k' \in \mathcal{K} \subset H^1(\mathcal{I})$. To show differentiability of the map $k \to T(\cdot;k)$ we need to prove the existence of the Fréchet differential T', such that

$$\lim_{\|k'\|_{H^1(\mathcal{I})} \to 0} \frac{\|T(k+k') - T(k) - T'(k;k')\|_{L_2(\Sigma)}}{\|k'\|_{H^1(\mathcal{I})}} = 0. \tag{B.6}$$

For simplicity, we shall use the following notation

$$\mathcal{R} \triangleq T(k+k') - T(k) - T'(k;k'), \quad \check{T} \triangleq T + T' + \mathcal{R}, \quad \delta T \triangleq T' + \mathcal{R}. \tag{B.7}$$

Writing equation (B.5) for $\check{T}$ and T, and subtracting we obtain

$$\int_\Omega \left[V(\check{T}) - V(T)\right] w\,d\mathbf{x} = -\int_\Omega V'(\check{T})\,w\,d\mathbf{x}, \tag{B.8}$$

where, in analogy with (15), the integrand on the RHS is defined as

$$V'(\check{T}) = \int_{T_\alpha}^{\check{T}} k'(s)\,ds$$

so that $V(\check{T}) = V(T) - V'(\check{T})$. Next, we postulate that the Fréchet differential T' satisfy the following equation

$$\int_\Omega k(T)\, T'\, w\, d\mathbf{x} = -\int_\Omega V'(T)\, w\, d\mathbf{x}. \tag{B.9}$$

Existence of solutions of (B.9) is established via a straightforward application of Lax–Milgram lemma, since (B.9) is a linear elliptic boundary–value problem. Therefore, our goal now is to prove that $\|\mathcal{R}\|_{L_2(\Sigma)}$, cf. (B.7), vanishes faster that $\|k'\|_{H^1(\mathcal{I})}$. Subtracting (B.9) from (B.8) yields

$$\int_\Omega \Big[V(\check{T}) - V(T) - k(T)\, T'\Big]\, w\, d\mathbf{x} = -\int_\Omega \Big[V'(\check{T}) - V'(T)\Big]\, w\, d\mathbf{x}. \tag{B.10}$$

Since $k(T) \in H^1(\mathcal{I})$, it follows from Taylor's theorem that there exist $\theta \in [0,1]$ such that

$$V(\check{T}) = V(T) + k(T)\, \delta T + \frac{1}{2}\dot{k}(T + \theta\delta T)(\delta T)^2, \tag{B.11}$$

almost everywhere in $\mathcal{T}$, where $\dot{k}$ denotes the derivative of k with respect to its argument. Therefore, the left hand side of (B.10) simplifies to

$$\int_\Omega \Big[k(T)\, \mathcal{R} + \frac{1}{2}\, \dot{k}(T + \theta\, \delta T)(\delta T)^2\Big]\, w\, d\mathbf{x}, \tag{B.12}$$

whereas for the right hand side of (B.10) we use

$$V'(\check{T}) = V'(T) + k'(T + \theta'\, \delta T)\delta T, \tag{B.13}$$

where $\theta' \in [0,1]$. Transforming equation (B.10) with expressions (B.12) and (B.13) yields

$$\int_\Omega k(T)\, \mathcal{R}\, w\, d\mathbf{x} = -\int_\Omega \Big[\frac{1}{2}\, \dot{k}(T + \theta\delta T)(\delta T)^2 + k'(T + \theta'\delta T)\delta T\Big]\, w\, d\mathbf{x}. \tag{B.14}$$

This is a linear elliptic boundary–value problem for which there exist an *a priori* estimate (see, for example, Section 2.3 in [36])

$$\|\mathcal{R}\|_{L_2(\Omega)} \leqslant \Big\|\frac{1}{2}\, \dot{k}(T + \theta\delta T)(\delta T)^2 + k'(T + \theta'\delta T)\delta T\Big\|_{L_2(\Omega)}. \tag{B.15}$$

For $k \in \mathcal{K}$ we can reduce inequality (B.15) to the form

$$\|\mathcal{R}\|_{L_2(\Omega)} \leqslant C_1 \|(\delta T)^2\|_{L_2(\Omega)} + \|k'\|_{L_2(\mathcal{I})}\, \|\delta T\|_{L_2(\Omega)}. \tag{B.16}$$

We now proceed to demonstrate that the RHS of (B.16) vanishes faster than $\|k'\|_{H^1(\mathcal{I})}$, i.e., as $\|k'\|^q_{H^1(\mathcal{I})}$ for some $q > 1$. In relation (B.16) and hereafter the symbols C with subscripts and primes will denote different positive constants.

We start with the term $\|\delta T\|_{L_2(\Omega)}$. Writing the original weak form (B.4) for k and $\check{k}$, subtracting and setting $u = \delta T$ produces

$$\int_\Omega \check{k}(\check{T})\, (\nabla\delta T)^2\, d\mathbf{x} + \int_\Omega \Big[k(\check{T}) + k'(\check{T}) - k(T)\Big]\, \nabla\delta T \cdot \nabla T\, d\mathbf{x} = 0. \tag{B.17}$$

For $\check{k} \in \mathcal{K}$ we have the following estimate for the first term in (B.17)

$$\int_\Omega \check{k}(\check{T})\,(\nabla\delta T)^2\,d\mathbf{x} \geqslant m_k\,\|\nabla\delta T\|^2_{L_2(\Omega)}. \tag{B.18}$$

Now we need to assume that $C_2 = \|\nabla T\|_{L^\infty(\Omega)} < \infty$, cf. [6]. Then, for the second term in (B.17) we have

$$\int_\Omega \Big[k'(\check{T}) + \dot{k}(T+\theta\delta T)\delta T\Big]\,\nabla\delta T\cdot\nabla T\,d\mathbf{x} \leqslant C_2\int_\Omega \Big[k'(\check{T}) + \dot{k}(T+\theta\,\delta T)\delta T\Big]\,|\nabla\delta T|\,d\mathbf{x}. \tag{B.19}$$

Next, we combine (B.18) and (B.19) to obtain the inequality

$$m_k\,\|\nabla\delta T\|_{L_2(\Omega)} \leqslant C_1'\,\|k'\|_{L_2(\mathcal{I})} + C_2'\,\|\delta T\|_{L_2(\Omega)}. \tag{B.20}$$

Using the following Poincare inequality $\|\delta T\|_{L_2(\Omega)} \leqslant C_3\|\nabla\delta T\|_{L_2(\Omega)}$ we see that

$$\frac{m_k}{C_3}\|\delta T\|_{L_2(\Omega)} \leqslant C_1'\|k'\|_{L_2(\mathcal{I})} + C_2'\|\delta T\|_{L_2(\Omega)}, \quad m_k\,\|\nabla\delta T\|_{L_2(\Omega)} \leqslant C_1'\,\|k'\|_{L_2(\mathcal{I})} + C_2'\,C_3\,\|\nabla\delta T\|_{L_2(\Omega)}.$$

Assuming that m_k is sufficiently large, so that $m_k - C_2'\,C_3 > 0$, we obtain

$$\|\delta T\|_{L_2(\Omega)} \leqslant \frac{C_1'\,C_3}{m_k - C_2'\,C_3}\,\|k'\|_{L_2(\mathcal{I})}, \quad \|\nabla\delta T\|_{L_2(\Omega)} \leqslant \frac{C_1'}{m_k - C_2'\,C_3}\,\|k'\|_{L_2(\mathcal{I})}. \tag{B.21}$$

Next we estimate $\|(\delta T)^2\|_{L_2(\Omega)} \equiv \|\delta T\|^2_{L_4(\Omega)}$. As a consequence of the Sobolev embedding theorem (see, e.g., Theorem 4.12 in [37]), we have the following inclusion

$$\mathcal{T} \subset H^1(\Omega) = W^{1,2}(\Omega) \subset L_6(\Omega), \quad n \leqslant 3.$$

Therefore, for $\delta T \in \mathcal{T}$ and in the light of estimates (B.21), we obtain

$$\|\delta T\|_{L_6(\Omega)} \leqslant C\,\|\delta T\|_{H^1(\Omega)} \leqslant C'\|k'\|_{L_2(\mathcal{I})}. \tag{B.22}$$

We then use the interpolation theorem (see e.g., Theorem 2.11 in [37]) for the L_p spaces which states that for $\xi \in L_p \cap L_q$, $1 \leqslant p \leqslant r \leqslant q \leqslant \infty$ and $t \in [0,1]$, we have

$$\|\xi\|_{L_r} \leqslant \|\xi\|^t_{L_p}\,\|\xi\|^{1-t}_{L_q} \quad \Longleftrightarrow \quad \frac{1}{r} = \frac{t}{p} + \frac{1-t}{q}.$$

Applying this result to $\|\delta T\|^2_{L_4(\Omega)}$ with $r = 4, p = 2, q = 6$ we obtain using (B.21) and (B.22)

$$\|\delta T\|_{L_4(\Omega)} \leqslant \|\delta T\|^{\frac{1}{4}}_{L_2(\Omega)}\,\|\delta T\|^{\frac{3}{4}}_{L_6(\Omega)} \quad \Longrightarrow \quad \|(\delta T)^2\|_{L_2(\Omega)} = \|\delta T\|^2_{L_4(\Omega)} \leqslant C''\|k'\|^2_{L_2(\mathcal{I})}. \tag{B.23}$$

Finally, substituting estimates (B.21) and (B.23) for $\|\delta T\|_{L_2(\Omega)}$ and $\|(\delta T)^2\|_{L_2(\Omega)}$ into (B.16) we obtain

$$\|\mathcal{R}\|_{L_2(\Omega)} \leqslant C_1\,\|(\delta T)^2\|_{L_2(\Omega)} + \|k'\|_{L_2(\mathcal{I})}\,\|\delta T\|_{L_2(\Omega)} \leqslant C'''\,\|k'\|^2_{L_2(\mathcal{I})} \leqslant C''''\,\|k'\|^2_{H^1(\mathcal{I})}, \tag{B.24}$$

This demonstrates that $\|\mathcal{R}\|_{L_2(\Omega)}$ vanishes faster than $\|k'\|_{H^1(\mathcal{I})}$. Therefore $k \longrightarrow T(\cdot;k)$ is Fréchet–differentiable from $H^1(\mathcal{I})$ to $L_2(\Sigma)$. □

We remark that, as is evident from (B.24), $T(\cdot; k)$ is also differentiable from $L_2(\mathcal{I})$ to $L_2(\Sigma)$.

References

[1] O. Volkov, B. Protas, W. Liao and D. Glander, "Adjoint–Based Optimization of Thermo–Fluid Phenomena in Welding Processes", *Journal of Engineering Mathematics*, **65**, 201–220, 2009.

[2] H. Banks and K. Kunisch, *Estimation techniques for distributed parameter systems*, Birkhäuser (1989).

[3] A. Tarantola, *Inverse Problem Theory and Methods for Model Parameter Estimation*, SIAM (2005).

[4] M. Z. Nashed and O. Scherzer, *Inverse problems, image analysis, and medical imaging*, AMS (2002).

[5] J. Gottlieb and P. DuChateau, *Parameter identification and inverse problems in hydrology, geology, and ecology*, Kluwer Academic Publishers (1996)

[6] G. Chavent and P. Lemonnier, "Identification de la Non–Linearité D'Une Équation Parabolique Quasilineaire", *Applied Mathematics and Optimization* **1**, 121–162, (1974).

[7] O. M. Alifanov, A. V. Nenarokomov, S. A. Budnik, V. V. Michailov and V. M. Ydin, "Identification of Thermal Properties of Materials with Applications for Spacecraft Structures", *Inverse Problems in Science and Engineering* **12**, 579–594, (2004).

[8] O. M. Alifanov, S. A. Budnik, V. V. Michaylov, A. V. Nenarokomov, D. M. Titov, and V. M. Ydin, "An experimental–computational system for materials thermal properties determination and its application for spacecraft structures testing", *Acta Astronautica* **61**, 341–451, (2007).

[9] X.-C. Tai and T. Kärkkäinen, "Identification of a Nonlinear Parameter in a Parabolic Equation from a Linear Equation", *Computational and Applied Mathematics* **14**, 157–184, (1995).

[10] P. DuChateau, R. Thelwell and G. Butters, "Analysis of an Adjoint Problem Approach to the Identification of an Unknown Diffusion Coefficient", *Inverse Problems*, **20**, 601–625, (2004).

[11] M. Janicki and S. Kindermann, "Recovering temperature dependence of heat transfer coefficient in electronic circuits", *Inverse Problems in Science and Engineering* **17**, 1129–1142, (2009).

[12] M. Hanke and O. Scherzer, "Error Analysis of an Equation Error Method for the Identification of the Diffusion Coefficient in a Quasi-Linear Parabolic Differential Equation" , *SIAM J. Appl. Math.* **59** 1012–1027, (1999).

[13] Ph. Kügler, *Identification of a Temperature Dependent Heat Conductivity by Tikhonov Regularization*, Diploma Thesis, Johannes Kepler Universität Linz (2000).

[14] Ph. Kügler, "Identification of a Temperature Dependent Heat Conductivity from Single Boundary Measurements", *SIAM J. Numer. Anal.* **41**, 1543–1563, (2003).

[15] A. Neubauer, "Identification of a Temperature Dependent Heat Conductivity via Adaptive Grid Regularization", *Journal of Integral Equations and Applications* **20**, 229–242, (2008).

[16] J.R. Cannon and P. DuChateau, "An Inverse Problem for a Nonlinear Diffusion Equation", *SIAM J. Appl. Math.* **39**, 272–289, (1980).

[17] P. DuChateau, "An Inverse Problem for the Hydraulic Properties of Porous Media", *SIAM J. Math. Anal.* **28**, 611–632, (1997).

[18] D. Luo, L. He, S. Lin, T.–F. Chen, and D. Gao, "Determination of Temperature Dependent Thermal Conductivity by Solving IHCP in Infinite Regions", *Int. Comm. Heat Mass Transfer* **30**, 903–908, (2003).

[19] L. T. Biegler, O. Ghattas, M. Heinkenschloss, D. Keyes, and B. van Bloemen Waanders, *Real–time PDE–constrained Optimization*, SIAM (2007).

[20] M. D. Gunzburger, *Perspectives in flow control and optimization*, SIAM (2003).

[21] W. Muschik, "Aspects of Non-Equilibrium Thermodynamics", World Scientific, (1989).

[22] B. D. Coleman and W. Noll, "The thermodynamics of elastic materials with heat conduction and viscosity", *Arch. Rat. Mech. Anal* **13**, 167–178, (1963).

[23] I.-S. Liu, "Method of Lagrange multipliers for exploitation of the entropy principle", *Arch. Rat. Mech. Anal* **46**, 131–148, (1972).

[24] V. Triano, Ch. Papenfuss, V. A. Cimmelli, and W. Muschik, "Exploitation of the Second Law: Coleman–Noll and Liu Procedure in Comparison", *J. Non-Equilib. Thermodyn.* **33**, 47–60, (2008).

[25] D. Luenberger, *Optimization by Vector Space Methods*, John Wiley and Sons (1969).

[26] J. Nocedal and S. Wright, *Numerical Optimization*, Springer (2002).

[27] A. Ruszczyński, *Nonlinear Optimization*, Princeton University Press (2006).

[28] C. R. Vogel, *Computational Methods for Inverse Problems*, SIAM (2002).

[29] G. Kirchhoff, *Vorlesungen über die Theorie der Warme*, Barth, Leipzig (1894).

[30] M. S. Berger, *Nonlinearity and Functional Analysis*, Academic Press (1977).

[31] J. Neuberger, *Sobolev Gradients and Differential Equations*, Springer (1997).

[32] B. Protas, T. Bewley and G. Hagen, "A comprehensive framework for the regularization of adjoint analysis in multiscale PDE systems", *Journal of Computational Physics* **195** (1), 49-89, (2004).

[33] B. Protas, "Adjoint–Based Optimization of PDE Systems with Alternative Gradients", *Journal of Computational Physics* **227**, 6490–6510, (2008).

[34] H. Engl, M. Hanke and A. Neubauer, *Regularization of Inverse Problems*, Kluver (1996).

[35] C. Homescu, I. M. Navon and Z. Li, "Suppression of vortex shedding for flow around a circular cylinder using optimal control", *Int. J. Numer. Meth. Fluids* **38**, 43–69, (2002).

[36] P. Grisvard, *Elliptic Problems in Nonsmooth Domains*, Pitman Publishing (1985).

[37] R. A. Adams, *Sobolev Spaces*, Academic Press, (1975).